MICROCOPY RESOLUTION TEST CHART
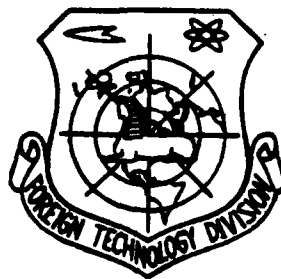NATIONAL BUREAU OF STANDARDS-1963-A

FOREIGN TECHNOLOGY DIVISION

JOURNAL OF ENGINEERING THERMOPHYSICS

(Selected Articles)

DTIC
SELECTE
OCT 4 1983

A

83 10 01 008

EDITED TRANSLATION

FTD-ID(RS)T-0285-83   13 September 1983

MICROFICHE NR: FTD-83-C-001136

JOURNAL OF ENGINEERING THERMOPHYSICS (Selected
Articles)

English pages: 64

Source: Gongcheng Rewuli Xuebao, Vol. 3, Nr. 4,
         November 1982, pp. 323-336; 346-356;
         361-364; 403-409

Country of origin: China
Translated by: LEO KANNER ASSOCIATES
                F33657-81-D-0264
Requester: FTD/TQTA
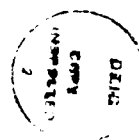Approved for public release; distribution unlimited.

TABLE OF CONTENTS

GRAPHICS DISCLAIMER

All figures, graphics, tables, equations, etc. merged into this
translation were extracted from the best quality copy available.

ii

THERMODYNAMIC EXTRAPOLATION OF ROCKET ENGINE PERFORMANCE PARAMETERS

Ge Minglong

Abstract

In this paper, extrapolation formulas of rocket engine performance parameters are established utilizing one isentropic reference line and two partial derivatives for fixed enthalpy. These formulas can be used for the extrapolation calculations of some parameters such as specific thrust, characteristic velicity, nozzle area ratio, and the thermodynamic parameters at the combustion chamber and the nozzle exit when changes occur in the initial enthalpy of the propellant, combustion chamber pressure and nozzle exit pressure. The formulas in this paper are simple, convenient to use and have relatively high accuracy.

I. INTRODUCTION

Methods of thermodynamic calculation of the theoretical performance of rocket engines are classic. These are introduced in reference 1 and other literature dealing with rocket engines. These diverse calculations are very useful for rocket engine design, but consume quite a lot of machine time. It is also inconvenient to put a large quantity of data into book form. Therefore, the problem of a calculation method for thermodynamic extrapolation of theoretical performance parameters of rocket engines is one that has been raised for a long time. Formulas for the calculation of thermodynamic extrapolation have been presented [2-5].

In recent years, with the popularity of pocket calculators, it has become more convenient to use extrapolation to determine the theoretical performance of rocket engines. This paper, therefore, proposes a more accurate extrapolation formula based on existing extrapolation formulas.

1

II. ISENTROPIC REFERENCE LINES

For the mixing ration O/F is any propellant composition with a definite value. Because its element composition is fixed, no matter what the numerical values (H_{co} or H_c) of the initial enthalpy of the propellant affected by such factors as ambient temperature and regardless of adopting a combustion chamber pressure (p_{co}, $p_{c'}$ or P_c) which is too high, and a nozzle exit pressure (p_{co}, $p_{c'}$, $p_{c''}$ or p_c) which is too high, the ideal thermodynamic process of a rocket engine ------- the isentropic limiting equilibrium expansion process, can both be shown as different isentropic lines $c_o t_o e_o e''$, cte,... etc. on the same enthalpy-entropy diagram, as shown in fig. 1.

For the initial enthalpy value of given propellants (H_{co}) and combustion chamber pressure (p_{co}), the thermodynamic parameters of the combustion chamber state point c_o and the throat state point t_o can be determined through accurate thermodynamic calculation. Several nozzle exit pressures are then selected and the thermodynamic parameters of these nozzle exit state points (c_o, c'',...) are calculated on the basis of isentropic conditions.

On isentropic line $c_o t_o e_o c''$, there are several points with known values for the parameters of pressure ratio p_c/p, pressure p, temperature T, enthalpy H, molecular weight M, constant pressure specific heat c_p and the values for the partial derivatives $\left(\frac{\partial \ln M}{\partial \ln p}\right)_T$, $\left(\frac{\partial \ln M}{\partial \ln T}\right)_p$ (see references 1 and 4 for the computation formulas and method of these two partial derivatives). This isentropic line can therefore become the reference line for extrapolation calculations. The parameters of a typical isentropic reference line are given in Table 1. The parameters given in the top half of this table are taken from reference 5.

On an isentropic reference line, apart from the known parametric points, the thermodynamic parameters of each point can

2

approximately be calculated by using the following interpolation formulas:

$$F = Q\ln p$$
$$(\Delta F)_s = Q(\Delta \ln p)_s$$ (1)

In the formulas, F expresses the parameters T,H,M etc., Q is the interpolation coefficient determined on the basis of the parameters of the two adjacent known points.

For the isentropic reference line in Table 1, the results of the calculation of the interpolation coefficients Q_T, Q_M and Q_H are given in the lower half of the table.

III. ISENTHALPIC PARTIAL DERIVATIVES AND ISENTHALPIC RELATIONAL EXPRESSIONS

By referring to related formulas given in references 4 and 5, the following formulas are used to express the two isenthalpic partial derivatives in this paper:

$$D_T = \left(\frac{\partial \ln T}{\partial \ln p}\right)_H = \frac{-R}{c_p M}\left(\frac{\partial \ln M}{\partial \ln T}\right)_p$$ (2)

$$D_M = \left(\frac{\partial \ln M}{\partial \ln p}\right)_H = \frac{-R}{c_p M}\left(\frac{\partial \ln M}{\partial \ln T}\right)_p^2 + \left(\frac{\partial \ln M}{\partial \ln p}\right)_T$$ (3)

In the formulas, R is a general gas constant (1.98726 Kcal/Kg mole K).

For the isentropic reference line in Table 1, the values of D_T, D_M, Q_{DT} and Q_{DM} which were calculated by using the above expressions are listed in the lower half of the table.

The relational expressions of temperature and molecular weight on the isenthalpic line are

$$(\Delta \ln T)_H = D_T(\Delta \ln p)_H$$ (4)

$$(\Delta \ln M)_H = D_M(\Delta \ln p)_H$$ (5)

3

By substituting the expression of the first law of thermodynamics and the state equation in the differential expression of entropy, we obtain

$$ds = \frac{dH}{T} - \frac{R}{M}\frac{dp}{p}$$

For the isenthalpic line (dH=0), from this expression we obtain

$$(\Delta s)_H = -\frac{R}{M}(\Delta \ln p)_H \qquad (6)$$

IV. THE ESTABLISHMENT OF AN EXTRAPOLATION FORMULA

1. Combustion Chamber Thermodynamic Parameters and Characteristic Velocity Formula

When the propellant initial enthalpy $H_c \neq H_{co}$ and combustion chamber pressure $p_c \neq p_{co}$, the parameters for c' in fig. 1 can be calculated from formula (1) based on known data from $\Delta H_c = H_c - H_{co}$ and point c_o. The parameters of point c can then be calculated from formulas (4) and (5) based on the parameters of point c' and $p = p_c$.

As a result, the formulas for combustion chamber temperature and molecular weight are obtained

$$T_c = \left(T_{co} + \frac{Q_H \Delta H_t}{Q_H}\right) \exp\left[\left(D_{Tco} + \frac{Q_{HT}\Delta H_t}{Q_H}\right)\left(\ln\frac{p_c}{p_{co}} - \frac{\Delta H_t}{Q_H}\right)\right] \qquad (7)$$

$$M_c = \left(M_{co} + \frac{Q_M \Delta H_t}{Q_M}\right)\exp\left[\left(D_{Mco} + \frac{Q_{HM}\Delta H_t}{Q_M}\right)\left(\ln\frac{p_c}{p_{co}} - \frac{}{}\right)\right] \qquad (8)$$

Because the characteristic velocity c* forms a direct ratio with $\sqrt{T_c/M_c}$, the extrapolation formula of the characteristic velocity can be written as

$$c^* = c_o^* \sqrt{T_c M_{co}/M_c T_{co}} \qquad (9)$$

4

2. Formula of Nozzle Exit ($p=p_c$) Thermodynamic Parameters

Formula (6) is applied between c and c' and between e and e':

$$\ln \frac{p_{c'}}{p_c} = \frac{M_{c'}}{M_{c'}} \ln \frac{p_{c'}}{p_c}$$

By substituting formula (1) into this expression, we obtain

$$\ln \frac{p_{c'}}{p_{co}} = \ln \frac{p_c}{p_{co}} + \frac{M_{co}\left(\frac{\Delta H_c}{Q_H} - \ln \frac{p_c}{p_{co}}\right)}{M_{co} + \frac{Q_M \Delta H_c}{Q_H}} \tag{10}$$

In the formula, M_{co} is the approximate value of $M_{c'}$. It is the known molecular weight of point $p=p_{co}$ near $p_{c'}$ on the isentropic reference line. The initial value of $p_{c'}$ can be calculated using the following expression in order to select p_{co} so as to determine M_{co}:

$$p_{c'o} = p_c \exp\left[\frac{M_{c''}}{M_{co}}\left(\frac{\Delta H_c}{Q_H} - \ln \frac{p_c}{p_{co}}\right)\right] \tag{11}$$

Key: (1) Initial.

This expression is approximately obtained from formula (10), where $M_{c''}$ is the known molecular weight of the lowest point of the isentropic reference line.

The interpolation coefficients Q_T, Q_{DT}, Q_M, Q_{DM} and Q_H in formulas (7), (8), (10) and (11) use values in the vicinity of p_{co}. When $\Delta H_c < 0$, the mean value of c_o-t_o is used and when $\Delta H_c > 0$, the value of $p > p_{co}$ is used.

On the basis of the known data of e_o and the value of $\ln\frac{p_{c'}}{p_{co}}$ calculated from formula (10), the parameters of point e' can be calculated from formula (1). On the basis of the parameters of e' and $p=p_c$, the parameters of point c can then be calculated from formulas (4) and (5). As a result, the nozzle exit temperature and molecular weight formulas are obtained

5

$$T_c = \left(T_{co} + Q_T \ln \frac{p_c'}{p_{co}}\right) \exp\left[\left(D_{Tco} + Q_{DT}\ln \frac{p_c'}{p_{co}}\right)\left(\ln \frac{p_c}{p_{co}} - \ln \frac{p_c'}{p_{co}}\right)\right] \quad (12)$$

$$M_c = \left(M_{co} + Q_M \ln \frac{p_c'}{p_{co}}\right) \exp\left[\left(D_{Mco} + Q_{DM}\ln \frac{p_c'}{p_{co}}\right)\left(\ln \frac{p_c}{p_{co}} - \ln \frac{p_c'}{p_{co}}\right)\right] \quad (13)$$

3. Formula of Specific Thrust Parameters

By substituting $H_c = H_{c'} = H_{co} + \Delta H_c$ and $H_c = H_{c'} = H_{co} + Q_H \ln \dfrac{p_c'}{p_{co}}$

in the design altitude specific thrust formula
$I = 294.98 \sqrt{(H_c - H_c)/1000}$, we obtain

$$I = 9.328 \sqrt{H_{co} + \Delta H_c - H_{co} - Q_H \ln \frac{p_c'}{p_{co}}} \qquad (14)$$

The interpolation coefficients Q_T, Q_{DT}, Q_M, Q_{DM} and Q_H in formulas (12) to (14) use values in the vicinity of p_{co}. When $\ln \dfrac{p_c'}{p_{co}} < 0$, values smaller than p_{co} are used; when $\ln \dfrac{p_c'}{p_{co}} > 0$ values are greater than p_{co} are used.

The nozzle exit ratio area and nozzle area ratio are calculated by the following formulas:

$$f_c = 86.50 T_c / I p_c M_c \qquad (15)$$
$$\varepsilon = f_c g p_c / c^* \qquad (16)$$

V. ACCURACY OF EXTRAPOLATION FORMULAS

Extrapolation calculations can be carried out according to the above formulas. The results of a number of extrapolation calculations for oxygen-hydrogen propellant with a mixing ratio O/F=7.9365, the nozzle area ratio, characteristic velocity, combustion chamber temperature and design altitude specific thrust are given n Tabl 2, 3 and Fig. 2 respectively. For comparison, the corresponding results of exact calculations [5,6] and the results of extrapolation calculations from reference 5 are also given.

6

From tables 2-4 and fig. 2 it can be seen that the accuracy of the extrapolation formulas of this paper is relatively high and can be suitably used for extrapolation calculations of the actual parametric range of rocket engines.

Table 1. Parameters on isentropic reference line (gas hydrogen gas oxygen propellant, mixing ratio O/F=7.9365 initial enthalpy H_{co}=0 Kcal/Kg).

量 (2)	(3)		(4)									
p_k/p	1	1.727	10	40.827	60.046	100	300	400	600	800	1000	3000	10000
p, 公斤/厘米²(绝对) (5)	68.05	39.40	6.805	1.667	1	0.6805	0.2268	0.1701	0.1134	0.0851	0.0680		0.0068
T, K	3600	3506	3015	2674	2556	2469	2218	2151	2055	1985	1930		1345
H, 大卡/公斤 (6)	0	−245.9	−942.0	−1412.1	−1566.2	−1676.9	−1968.2	−2038.7	−2133.9	−2198.6	−2247.1		−2663.7
M, 公斤/公斤克尔 (7)	15.752	15.974	16.656	17.148	17.310	17.423	17.702	17.761	17.834	17.878	17.907		18.014
c_p, 大卡/公斤 K (8)	2.5901	2.5481	2.2704	1.9066	1.7508	1.6279	1.2694	1.1787	1.0577	0.9784	0.9217		0.6126
$\left(\frac{\partial \ln M}{\partial \ln p}\right)_T$	0.05008	0.04509	0.02958	0.01844	0.01484	0.01234	0.00633	0.00508	0.00358	0.00270	0.00212		0.00004
$\left(\frac{\partial \ln M}{\partial \ln T}\right)_p$	−0.8458	−0.8081	−0.6118	−0.4308	−0.3630	−0.3125	−0.1786	−0.1479	−0.1090	−0.0849	−0.0606	−0.0173	−0.0018
$D_T = \left(\frac{\partial \ln T}{\partial \ln p}\right)_H$	0.04120	0.03906	0.03215	0.02619	0.02380	0.02190	0.01579	0.01404	0.01148	0.00965	0.00826		0.00032
$D_M = \left(\frac{\partial \ln M}{\partial \ln p}\right)_H$	0.01523	0.01384	0.00991	0.00716	0.00620	0.00550	0.00351	0.00300	0.00233	0.00188	0.00155		0.00004
$g_T = \left(\frac{\Delta T}{\Delta \ln p}\right)_i$	357⁰	318.4	279.6	242.4	230.9	226.0	228.4	232.9	236.8	243.8	245.2	255.2	253.0
$g_M = \left(\frac{\Delta M}{\Delta \ln p}\right)_i$	−0.424⁰	−0.4062	−0.3884	−0.3490	−0.3170	−0.2936	−0.2539	−0.2051	−0.1800	−0.1533	−0.1293	−0.0775	−0.0183
$g_H = \left(\frac{\Delta H}{\Delta \ln p}\right)_i$	504⁰	450.0	396.4	334.2	301.5	287.6	265.1	245.1	234.8	225.4	216.2	198.5	164.9
$g_{DT} = \left(\frac{\Delta D_T}{\Delta \ln p}\right)_i$			0.003935	0.004237	0.004677	0.004936	0.005561	0.006083			0.006197		0.001950
$g_{DM} = \left(\frac{\Delta D_M}{\Delta \ln p}\right)_i$				0.001955	0.001875	0.001815	0.001811	0.001773	0.001652	0.001567	0.001471		0.000307

* 外插公式外推值 (9)

Fig. 1   Enthalpy-entropy schematic
diagram.

Key: (1) Enthalpy;
     (2) Isentropic refer-
     ence line; (3) Entropy.
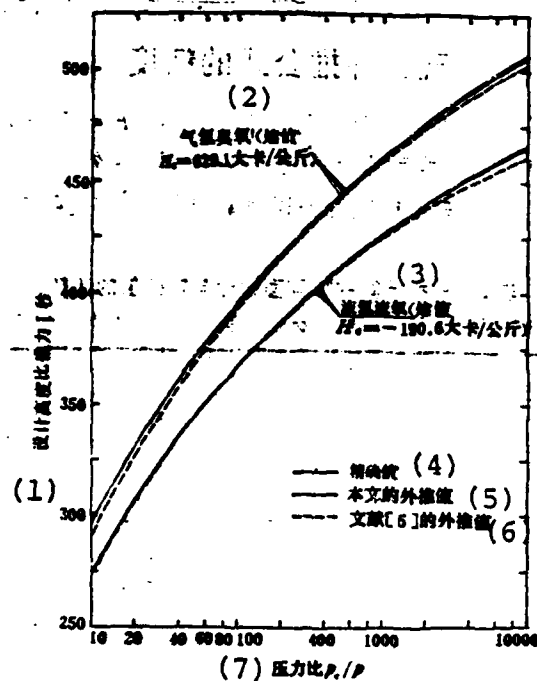
Fig. 2 Comparison of design altitude
specific thrust calculated by
extrapolation with exact value
(hydrogen-oxygen propellant, mixing
ratio O/F-7.9365, combustion chamber
pressure p_c=6.805 kg/cm^2,
absolute).

Key: (1) Design altitude specific
thrust I seconds; (2) Gas
hydrogen ozone (enthalpy H_c=
629.1 Kcal/kg); (3) Liquid
hydrogen liquid oxygen (enthalpy
H_c=190.6 Kcal/kg); (4) Exact
value; (5) Extrapolation value
of this paper; (6) Extrapolation
value of reference 5;
(7) Pressure ratio.

9

Table 2. Comparison of nozzle area ratio calculated by
extrapolation with exact values (hydrogen-
oxygen propellant, mixing ratio O/F=7.9365
combustion chamber pressure p_C=6.805 kg/cm^2
absolute)

p_c/p	(1) 被氧液氢, 焓值 H_c = −190.6 大卡/公斤			(2) 气氢臭氧, 焓值 H_c = 629.1 大卡/公斤		
	(3) 精确值	(4) 本文的外插值	(5) 文献5的外插值	(6) 精确值	(7) 本文的外插值	(8) 文献5的外插值
10	2.468	2.476	2.289	2.466	2.459	2.337
40.83	7.151	7.188	7.130	7.169	7.196	7.279
68.05	10.75	10.80	10.77	10.81	10.77	11.00
100	14.69	14.74	14.70	14.81	14.70	15.01
300	36.28	36.40	35.70	37.02	37.05	36.45
400	46.04	46.19	45.04	47.22	47.29	45.98
600	64.44	64.58	62.49	66.66	66.55	63.80
800	81.77	81.90	78.83	85.21	84.97	80.49
1000	98.31	98.41	94.40	103.2	103.6	96.38

Key: (1) Liquid oxygen liquid hydrogen, enthalpy H_C=190.6
Kcal/kg; (2) Gas hydrogen ozone, enthralpy H_C=629.1
Kcal/kg; (3) Exact value; (4) Extrapolation value of
this paper; (5) Extrapolation value of ref. 5;
(6) Exact value; (7) Extrapolation value of this paper;
(8) Extrapolation value of ref. 5.

(1) 燃烧室压力 p_c 公斤/厘米², 绝对	(2) 气氢气氧, 焓值 H_c = 0 大卡/公斤			(7) 液氢液氧, 焓值 H_c = −190.6 大卡/公斤			(12) 气氢臭氧, 焓值 H_c = 629.1 大卡/公斤		
	(3) 精确值	(4) 外插值		(8) 精确值	(9) 外插值		(13) 精确值	外插值 (14)	
		(5) 本文	(6) 文献5		(10) 本文	(11) 文献5		(15) 本文	(16) 文献5
68.05	2197	2197	2197	2156	2156	2157	2324	2326	2329
40.83	2184	2182	2184	2144	2142	2144	2308	2310	2316
6.805	2136	2132	2139	2099	2094	2099	2251	2254	2271

(17) 注: 表中特征速度数值的单位是米/秒

Table 3. Comparison of characteristic velocity calculated
by extrapolation with exact values (hydrogen-
hydrogen propellant, mixing ratio O/F-7.9365)

Key: (1) Combustion chamber pressure p_C, kg/cm^2, absolute;
(2) Gas hydrogen gas oxygen enthalpy H_C=0 Kcal/kg;
(3) Exact value; (4) Extrapolation value; (5) This
paper; (6) Reference 5; (7) Liquid hydrogen liquid
oxygen, enthalpy H_C=-190.6 Kcal/kg; (8) Exact value;
(9) Extrapolation value; (10) This paper; (11) Refer-
ence 5; (12) Gas hydrogen gas oxygen, enthalpy
H_C=629.1 Kcal/kg; (13) Exact value; (14) Extrapolation
value; (15) This paper; (16) Reference 5; (17) Note; in
this table, the unit for the characteristic velocity
values is m/sec.

10

Table 4. Comparison of combustion chamber temperature
calculated by extrapolation with exact values
(liquid hydrogen liquid oxygen propellant,
mixing ratio O/F-7.9365)

(1) 燃烧室压力 p_c公斤/厘米²，绝对	1.02	2.04	4.08	10.21	20.42	40.83	61.25	81.56
(2) 精确值	3039	3127	3217	3341	3437	3534	3591	3632
(3) 本文的外推值	3053	3138	3225	3344	3437	3533	3590	3631

(4) 注：表中燃烧室温度数值的单位是K

Key: (1) Combustion chamber pressure p_c kg/cm^2,
absolute; (2) Exact value; (3) Extrapolation
value of this paper; (4) Note: in this table,
the unit for the combustion chamber temperature
values is K.

References

[1] S. Gordon, F.J. Zeleznik, and V.N. Huff: A general method for
automatic computations of equilibrium compositions and
theoretical rocket performance of propellants, NASA TN D-132.
(October 1959).

[2] S. Gordon, and V.N. Huff: Theoretical performance of liquid
hydrazine and liquid fluorine as a rocket propellant, NACA
RM E53E12, (1953).

[3] L.J. Gordon: Uncertainty in a calculated specific impulse due
to an uncertainty in the heat of formation of the propellant,
ARS J. 30, (1960), 115-116.

[4] M. Barrere, et al: Rocket Propulsion (Chapter 3), Elsevier
Publishing Company, Amsterdam, London, New York. Princeton.
1960.

[5] S. Gordon, and F.J. Zeleznik: Thermodynamic extrapolation of
rocket performance parameters, ARS J.32, (1962) 1195-1202.

[6] G. K. Sievers, et al: Theoretical performance of hydrogen-
oxygen rocket: thrust chambers, NASA TR R-111. (1961).

A THERMODYNAMIC CALCULATION METHOD OF THE SYMBOLIC FORMULA FOR ROCKET ENGINES

Fang Zhaokui

Abstract

A symbolic element is substituted for chemical elements which cause practical chemical reaction. With the use of the symbolic formula, a new calcualtion method has been set up to calculate theoretical performance of the propellant. It will be able to devise a general computer program for chemical equilibrium of rocket engine, which does not depend on practical chemical element.

In the past, a chemical thermodynamic calculation method was widely used in China. Its special feature is that the chemical reaction formula must be correlated with the practical chemical elements of the propellant. It is therefore very difficult to design a general program. The symbolic thermodynamic calculation method proposed in this paper eliminates the above difficulty.

I. SYMBOLIC ELEMENTS AND THEIR MOLECULAR FORMULAS

We let a pair of positive integers i and j produce i types of propellants from combustion products for any element having j to define a group of symbolic elements as A_j and their corresponding symbolic element atomic number by a_j. The ordered permutation of symbolic element A_j is:

$$\prod^{j} A_{j}a_{ji} = A_{1}a_{1L} A_{2}a_{2i} \cdots A_{j}a_{ji} \quad (i = 1, 2, \cdots i) \qquad (1)$$

This expresses the molecula formula for i types of combustion products produced after propellant combustion. The symbol $\prod^{j}$ expresses the ordered permutation as in formula (1).

For example, for the four element propellants C, H, O and N, A_1, A_2, A_3, A_4 respectively are used as symbolic elements in their place. Letting i types of combustion products be CO, obviously, on the basis of this definition, its molecular formula for the symbolic elements is:

$$CO = \prod^j A_j a_{ji} = A_1 1 A_2 0 A_3 1 A_4 0 \qquad (2)$$

The relationship between the designational order i, j, and the products and elements is arbitrary. However, as soon as a relationship is assigned, formula (2) only determines CO.

II. A CHEMICAL EQUILIBRIUM EQUATION FOR SYMBOLIC ELEMENT COMBUSTION PRODUCTS

Definition: For any molecular combustion product $\prod^j A_j a_{ji}$, let the dissociation reaction of the correlation of the product and its symbolic element A_j

$$\prod^j A_j a_{ji} \rightleftharpoons \sum^j a_{ji} A_j \ (i = 1, 2 \cdots i) \qquad (3)$$

be a formula of a chemical equilibrium reaction. Because several partial factors are assigned to the symbolic elements, their corresponding conventional rules of multiplication:

$$a_{ji} \times A_j = \begin{cases} 0 & \text{If} \quad a_{ji} = 0 \\ a_{ji} A_j & \text{If} \quad a_{ji} \neq 0 \end{cases} \qquad (4)$$

By the theory of chemical equilibraium reaction, the corresponding chemical equilibrium equation for formula (3) will be:

$$P_{\prod^j A_j a_{ji}} \Big/ \left(P_{A_1}^{a_{1i}} \times P_{A_2}^{a_{2i}} \times \cdots \times P_{A_j}^{a_{ji}} \right) = f_i(T) \ (i = 1, 2 \cdots i) \qquad (5)$$

In the formula, $P_{\prod^j A_j a_{ji}}$, P_{A_j} respectively express the partial pressure of the symbolic element combustion product $\prod^j A_j a_{ji}$ and the atomic product A_j during the combustion process, $f_i(T)$ is the equilibrium constant of the dissociation reaction under

13

temperature T. If a certain element does not exist in this
molecule (e.g. there is no hydrogen in the CO molecule), then
because of the conventional mathematical law $p_{A_j}^0 = 1$, formula
(5) will inevitably be satisfied. From the left and right
sides of formula (5), the following logarithm can be obtained:

$$\ln P_j \frac{}{\prod^{a_{ji}}} = \ln f_i(T) + \sum a_{ji} \ln P_{A_j} \qquad (6)$$

By using formula (6), molecular partial pressure can be
converted into atomic partial pressure, molecular variables can
be eliminated and, furthermore, we can greatly decrease the
number of equations.

III. PROPELLANT MATRICES FOR SYMBOLIC ELEMENTS AND THEIR
      NORMALIZATION PROCESS

    Definition: If there is a type of complex propellant
composed from n types of pure chemical mixtures, each type is a
pure chemical molecular expression. When the percentage of heat
content and mixture weight is respectively $\prod A_j a_{jn}, H_n, x_n \ (n = 1, 2, \cdots n)$
then the characteristics of the propellant are completely
determined by the matrix

$$A(n, j+2) = \begin{pmatrix} a_{11} & a_{21} & \cdots & a_{j1} & H_1 & x_1 \\ a_{12} & a_{22} & \cdots & a_{j2} & H_2 & x_2 \\ \vdots & \vdots & & \vdots & \vdots & \vdots \\ a_{1n} & a_{2n} & \cdots & a_{jn} & H_n & x_n \end{pmatrix} \qquad (7)$$

Formula (7) is called the propellant matrix. In performance
computations, it is only necessary to consider the theoretical
performance possessed by the unit mass.

For this reason

Definition: The unit mole propellant symbolic element atomic formula which takes the molecular weight as 1 is the standardized equivalent formula of the propellant. The process of converting the original propellant into an equivalent formula for a symbolic element propellant is known as the symbolic element propellant normalization process.

Theorem: If there is a complex propellant (7), μ_j is the atomic weight of the symbolic element A_j, letting the matrix

$$B(n) = \begin{pmatrix} x_1 / \sum_j \mu_j a_{j1} \\ x_2 / \sum_j \mu_j a_{j2} \\ \vdots \\ x_n / \sum_j \mu_j a_{jn} \end{pmatrix} \qquad (8)$$

then the normalization process of propellant (7) is realized as the matrix operation of the following formula

$$A(j+1) = A'(n, j+1) \times B(n) = \begin{pmatrix} a_{10} \\ a_{20} \\ \vdots \\ a_{j0} \end{pmatrix} \qquad (9)$$

In the formula, A'(n,j+1) is the transposed matrix of A(n,j+1) obtained after taking out the final column from matrix (7). (9) is a column matrix after normalization. The subscript "0" of the column matrix element a_{j0} shows that it does not belong inside the combustion product serial number "i". From (9) we can deduce:

$$\sum_j \mu_j a_{j0} = 1 \qquad (10)$$

15

This is the inevitable result of normalization processing. For the double element liquid propellant, if the incendiary agents corresponding to the forms in (7) and (8) are A(n,j+2), B(n), the oxidant is A(m,j+2), B(m), and K is the mixing ratio. Therefore, the normalization process of this type of complex double element propellant is:

$$A(j+1) = [A'(n, j+1) \times B(n) + KA'(m, j+1) \times B(m)]/(1+K) \quad (11)$$

The final result is similarly a column matrix. (9), (10) and (11) are proof.

IV. A BASIC EQUATION AND PROGRAM DESIGN FOR THE THERMODYNAMIC CALCULATION OF THE SYMBOLIC FORMULA

Given the propellants determined by the positive integers i and j and the normalized matrix A(j+1), the standard formula for the combustion reaction is:

$$M \prod_i A_{i,a_{ji}} \longrightarrow \sum_i P_i \prod_i A_{i,a_{ji}} \quad (12)$$

The above formula expresses that the combustion product $\prod_i A_{i,a_{ji}}$ has partial pressure P_i separately produced by M mole propellants at the time of combustion. However, when there is a condensed phase, P_i should be seen as the number of moles of the condensed phase product. The four basic equations for the symbolic thermodynamic calculation are now changed to the following:

1. Equation of Mass Conservation:

$$a_{ji} = \sum_i a_{ji} P_i/M \quad j = 1, 2, \cdots j \quad (13)$$

2. Equation of Energy Conservation:

16

$$H_0 - \sum^i (H_T^0)_i P_i / M \qquad \text{(等焓-燃烧室状态)} \Big] (1)$$

$$S_0 - \sum^i [(S_T^0)_i - \beta_i] P_i / M \quad \text{(等熵-喷管状态)} \Big] (2) \qquad (14)$$

Key: (1) Isenthalpy-combustion
chamber state; (2) Isentropy-
nozzle state.

3. Equation of Chemical Equilibrium:

$$(F_T^0)_i / (RT) + \ln\omega_i - \sum^i a_{ji} [(F_T^0)_i / (RT) + \ln\omega_i] = 0 \quad i = 1, 2, \cdots i, \qquad (15)$$

In formulas (14) and (15), $(H_T^0)_i$, $(S_T^0)_i$ and $(F_T^0)_i$ are respec-
tively the enthalpy, entropy and free energy of i type products
at temperature T.

$$\beta_i = \begin{cases} R \ln P_i & \text{(for gas phase)} \\ 0 & \text{(for condensed phase)} \end{cases} \qquad \omega_i = \begin{cases} P_i & \text{(for gas phase)} \\ 1 & \text{(for condensed phase)} \end{cases}$$

R is a mole universal gas constant. The discriminants of the
solidifying phase are omitted.

4. Dalton's Law:

$$P_0 - \sum^i P_i \quad \text{(仅对气相)} \qquad (16)$$

Key: (1) Only for gas phase.

When A(n,j+2), A(m,j+2), K, P_0, H_0 and μ_j are already
known, a basic proposition of a thermodynamic calculation is
formed in seeking a solution to the above equation.

In program design, the system of equations must be linearized, and when using the reduced number of equation (6) the partial derivative approach and divergence factors are used to solve the problem of initial value arbitrariness within a wide range. We used BCY language to work out a general program for thermodynamic calculations of the symbolic formula and were successful in calculating logarithms on a 109 C machine for several tens of types of propellants. The above contents are limited in space but further details are not necessary.

References

[1] V.E. Alemasov, Principles of Rocket Engines, National Defense Industries Publications, 1965.

[2] B.J. McBride, S. Heimel, J.G. Ehlers, S. Gordon: "Thermodynamic Properties to 6000K for Substances Involving the First 18 Elements", NASA SP-3001, (1963).

A CORRECTED CALCULATION METHOD FOR ISENTROPICALLY EXPANDING PROCESSES OF COMBUSTION PRODUCTS OF HYDROCARBON WITH AIR

Yang Donghua

East China Institute of Chemical Technology

Abstract

In this paper an immediate and more accurate calculation method for isentropically expanding processes of combustion products of hydrocarbon with air is suggested. The accuracy of this method suggested by this paper is 4-9 times more accurate than the β_T number method [1] and the B_{CH_2} number method [1] while its computation is a little more laborious.

Three types of approximate calculations for isentropically expanding processes of non-standard combustion products are presented in reference [1]. A simpler and more exact calculation method for isentropically expanding processes of non-standard combustion products (limited to hydrocarbon combustion products) is proposed in this paper.

If
$$\varphi = \int_T^2 c_p dT \Big/ \int_1^2 c_{p_{CH_2}} dT$$

and
$$\phi = \int_1^{2l} (c_p/T) dT \Big/ \int_1^T (c_{p_{CH_2}}/T) dT$$

are introduced, then the non-standard combustion product is isentropically expanded from initial state 1 to final state 2. Its heat drops ΔI and $\Delta \lg \pi^o$ can be respectively corrected as:

$$\Delta I = \int_1^2 c_p dT = \varphi (\Delta I)_{CH_2} \text{ 和}$$

$$\Delta \lg \pi^o = \int_1^2 \frac{4.5725 c_p dT}{T} = \psi (\Delta \lg \pi^o)_{CH_2}.$$

Key: (1) And.

After coefficients φ and ψ have been corrected, it is convenient to directly use reference 2 and borrow the following steps to carry out the calculation:

$$\Delta \lg \pi^0 \longrightarrow (\Delta \lg \pi^0)_{CH_2} = (\Delta \lg \pi^0)/\psi \longrightarrow$$

$$(\pi_1^0/\pi_2^0)_{CH_2} = 10^{(\Delta \lg \pi^0)_{CH_2}} \quad \underline{\text{consult ref. 2 for calculations}}$$

T_{2*} $(\Delta l)_{CH_2} \longrightarrow \Delta l = \varphi(\Delta l)_{CH_2}$. However, if the above steps are used directly from reference 2 to carry out the calculations, it is first necessary to have calculated the corrected coefficients φ and ψ for the gases of the various combustion products and β numbers. However, for reasons given below, it is not necessary to first calculate the corrected coefficients for the gases of the various combustion products and β numbers one by one. This is because all the gases of the hydrocarbon combustion product CH_n with various β numbers can be viewed as being formed from the gas superposition of the C and CH_2 of the same β number:

$$(1 + 0.25n + 0.052476n\beta) \,(gas)_{\beta, CH_n} = (1 - 0.5n) \,(gas)_{\beta, C} + (0.75n + 0.052476n\beta) \,(gas)_{\beta, CH_2}$$

Therefore, we can obtain:

$$(gas)_{\beta, CH_n} = [A'/(A' + B')] \quad (gas)_{\beta, C} + [B'/(A' + B')] \,(gas)_{\beta, CH_2}$$

In the formula, $A' + 1 - 0.5n$; $B' = 0.75n + 0.052476n\beta$. In this way, after undergoing isentropic expansion, the corrected values φ_n^β and ψ_n^β of the gases of CH_n can be calculated by using the corrected values φ_0^β and ψ_0^β of the gases of C:

$$\varphi_n^\beta = (\Delta l_n^\beta/\Delta l_1^\beta) = (A'\varphi_0^\beta + B')/(A' + B'),$$
$$\psi_n^\beta = [(\Delta \lg \pi_n^\beta)/(\Delta \lg \pi_1^\beta)] = (A'\psi_0^\beta + B')/(A' + B')$$

20

Thus, provided we have the corrected values φ_0^β and ψ_0^β of all the gases of the β numbers of C, the isentropic processes of CH_n hydrocarbon with air combustion products can be directly calculated according to the steps described above and using the most exhaustive and up-to-date table of the thermodynamic properties of gases [2].

The author calculated the β numbers as 0.1, 0.2.....1.0 of the gases of C. Ten types of initial temperatures from 1500, 1400.....600°C etc. were isentropically expanded to the corrected coefficients φ_0^β and ψ_0^β of the ten final temperatures 1050, 850.....etc. From the results of the calculations, it can be seen that changes are slow for φ_0^β and ψ_0^β values in relation to initial and final temperatures. Therefore, this type of detailed table of corrected coefficients can be used satisfactorily for engineering calculations [3].

We later carried out an accuracy analysis of the calculations. From Table 1 it can be seen that the accuracy of the corrected calculations in this paper is: heat drop $\Delta I \leqslant 0.05\%$; final absolute temperature $T_2 \leqslant 0.1\%$. The accuracy was 5-10 times greater than the β_γ number method and the B_{CH_2} number method, although the calculations were slightly more complex.

Table 1

燃料 (a)	β	t_1℃	(c) 内容 \ t_2温℃	30	100	150	200	300	400	406.11	500	700	1100
H₂	1	1500	(d) 压力比 p_1/p_2	1100.5	646.3	405.0	267.15	129.08	69.06		39.76	15.33	3.35
			(e) △I确 大卡/公斤-莫尔	12352.1	11985.6	11616.7	11244.7	10489.8	9716.9		8923.3	7273.9	3753.0
			(f) △I 大卡/公斤-莫尔	12351.4	11985.2	11617.6	11244.5	10489.0	9715.3		8921.5	7272.5	3751.0
			t_2℃	50.04	100.14	150.00	200.11	300.13	400.23		500.13	699.58	1099.93
			△I%	0.006	0.003	−0.008	0.002	0.01	0.02		0.02	0.02	0.05
			T_2%	−0.01	−0.04	0	−0.02	−0.03	−0.03		−0.02	0.04	0.005
	1	1100	p_1/p_2	328.93	193.19	121.20	79.86	38.58	20.65		11.89	4.58	
			(g) △I确	8599.1	8232.6	7863.7	7491.7	6736.8	5963.9		5170.3	3520.9	
			△I	8597.7	8232.1	7862.7	7490.9	6735.4	5962.9		5169.8	3519.9	
			t_2	50.04	100.05	150.00	200.11	300.07	400.12	−	500.04	699.79	
			△I%	0.02	0.006	0.01	0.01	0.02	0.02		−0.01	0.03	
			T_2%	−0.01	−0.01	0	−0.02	−0.01	−0.02		−0.005	0.02	
	1	700	p_1/p_2	71.18	42.16	26.45	17.43	8.42	4.51		2.59		
			(h) △I确	5078.2	4711.7	4342.8	3970.8	3215.9	2443.0		1649.4		
			△I	5078.4	4711.7	4342.9	3970.5	3214.9	2441.9		1649.9		
			t_2	49.98	100.05	149.98	200.03	300.07	400.15		499.96		
			△I%	−0.004	0	−0.002	0.01	0.03	0.05		−0.03		
			T_2%	0.006	−0.01	0.004	−0.006	−0.01	−0.02		0.005		
CH₄	1	1500	p_1/p_2	1222.9	716.0	446.5	292.5	139.57	73.67		41.91		
			(i) △I确	12525.6	12156.2	11783.2	11405.9	10637.5	9848.5		9037.4		
			△I	12525.6	12156.8	11783.0	11405.5	10637.3	9847.2		9036.3		
			t_2	49.98	100.07	150.05	200.06	300.03	400.19		500.09		
			△I%	0	−0.005	−0.002	0.003	0.001	0.01		0.01		
			T_2%	0.006	−0.02	−0.01	−0.01	−0.005	−0.03		−0.01		
CH₃.₈₀₀	0.2	750	p_1/p_2							5			
			(j) △I确							2690.3			
			△I							2690.8			
			t_2							406.13			
			△I%							−0.019			
			T_2%							−0.003			
CH₄	0.2	1500	p_1/p_2	762.6	457.3	291.2	195.3	97.07	53.32		31.43		
			(k) △I确	11615.4	11262.7	10908.0	10550.8	9826.1	9085.5		8327.5		
			△I	11618.8	11264.0	10908.9	10551.2	9827.9	9085.9		8321.8		
			t_2	50.30	100.34	150.40	200.40	300.29	400.29		500.64		
			△I%	−0.03	−0.01	0.008	−0.004	−0.02	−0.006		0.07		
			T_2%	−0.09	−0.09	−0.09	−0.08	−0.05	−0.04		−0.08		

22

Table 1 Using the corrected calculation method in this paper, the following were calculated from each kind of initial temperature t_1°C: (gas) β=1,H_2, (gas) β=1,CH_4, (gas) β=0.2, $CH_{3.887}$, (gas) β=0.2,H_2, as well as the t_2°C and ΔI values and their relative errors $\Delta I\%$, $T_2\%$ after isentropic expansion of the fixed pressure ratio p_1/p_2.

Key: (a) Combustion product; (b) True; (c) Content; (d) Pressure ratio; (e) True Kcal/kg-mole; (f) True Kcal/kg-mole; (g) True; (h) True; (i) True; (j) True; (k) True.

References

[1] Yang Donghua: Calculation and Analysis of the Thermodynamic Properties of Gases, Journal of Mechanical Engineering, 16,4 (1980), 89-100.

[2] Wu Zhonghua: Table of the Thermodynamic Properties of Gases, 2nd edition, Science Publishing Co., Peking, 1959.

[3] Yang Donghua: (This paper) was read at the Conference on Thermodynamic Engineering and Power Economy jointly sponsored by the Chinese Engineering Thermophysics Institute and the Chinese Institute of Aeronautics, Oct., 1981.

THE EXPERIMENTAL INVESTIGATION OF THE TIP FLOWS IN DIFFUSER CASCADES

Lai Shengkai, Su Rongpei, Su Jiexian, Cheng Le and Jiao Deyong
Harbin Institute of Technology

Abstract

The results of the experimental investigation of tip flows in diffuser cascades are presented. The results of measurements of secondary flow velocities, main flow velocity, total pressure as well as air flow deflection angle in the vicinity of the end wall of the exit plane of the cascade are presented. The authors point out that the effects of the shrouding on the aerodynamic characteristics must be considered when inner shrouding is employed in compressor stationary cascades.

In order to determine the effect of movement of the end wall of an axial flow compressor stationary cascade on secondary flow, the authors carried out experimental investigation on a stationary cascade wind tunnel (M no. approx. 0.2). The experimental cascade consisted of circular arc straight vanes. In order to simulate an unshrouded cascade, a flat variable speed moving belt was substituted for the end wall surface of the experimental cascade. A five-hole probe was used to measure air flow.

Figures 1 and 2 each show the distribution of secondary flow velocity. In the figures, $\bar{W}_x$ is the component velocity along the direction of the cascade spacing; the direction toward the suction surface is positive; $\bar{W}_y$ is the component velocity along the direction of the blade height, and because of the end wall the direction toward the center is positive. $\bar{W}_x$ and $\bar{W}_y$ in the figures are both relative values of the main flow velocity W_{z0} for the same cascade spacing locations. v is the velocity of movement of the belt.

From the velocity distribution in figs. 1 and 2 it can be seen that the secondary flow is more or less a triangular shaped circulation region in the air passage. The effect of end wall movement on circulation is mainly produced within a relatively small region near the wall corner of the suction surface and the flow effects are small at some distance from the wall corner. When the end wall moves, the flow in the positive direction near the end wall is markedly weakened and the circulation region is reduced.

Figure 3 shows the distribution of mean flow direction vortices. Counterclockwise circulation is positive. The symbols " ● " and " △ " in the figures represent the vortex strength when the lower end wall of the cascade is stationary and when moving respectively. It can be seen from the figure that when the end wall is not moving, the vortex is strongest at area 1 near the wall corner of the suction surface. When it is moving, there is a general drop in vortex strength and the strongest vortices shift from area 1 to area 2.

From fig. 4 it can be seen that, apart from near the suction surface, the effect of the end wall movement on main flow velocity is very small. Near the wall corner of the suction surface there is a marked drop in main flow velocity when the end wall is not in motion. When the end wall is in motion, there is a relatively large change in main flow velocity near the wall corner of the suction surface and an increase of main flow velocity near the end wall.

The difference between the air flow deflection angle of the tip region and that of the main flow region is known as the air flow over-deflection angle. Figure 5 shows the distribution of over-deflection angles (a) and the mean value of the flow rates (b). The over-deflection angle is greater near the end wall of the suction surface and reaches a maximum of 15°. Because of the

25

over-deflection of the air flow, there is an increase in blade loading in this area and a deviation from the design values of cascade inlet angles. Therefore, the characteristics of the tip region should be considered in calculating the design of cascades. End wall motion can cause a clear reduction in the over-deflection angle in the wall corner region of the suction surface.

From fig. 6 it can be seen that flow loss is mainly concentrated in the area of two wall corners, especially the area of the wall corner of the suction surface. End wall motion causes a reduction in high loss areas.

Based on an analysis of the results of the experiment the following conclusions are obtained:

1. There is a lot of over-deflection of the flow in the wall corner region of the suction surface in compressor stationary cascades because of the presence of tip flows.

2. End wall motion can weaken secondary flow in the air passage as well as weaken the over-deflection of air flow in the wall corner region.

3. To know whether or not to use an inner shrouding in the stationary cascade in the design of compressors, it is necessary to make adequate allowance for the effect of the inner shrouding on air flow in the cascade.
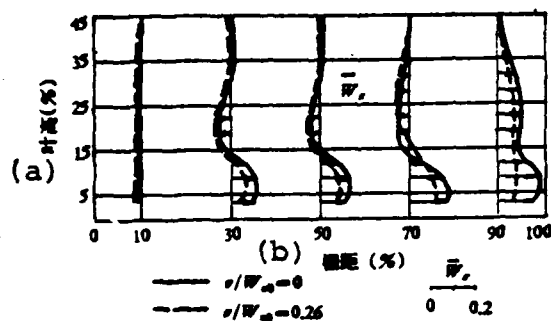
Fig. 1 Component velocity distribution in
in the direction of cascade spacing.

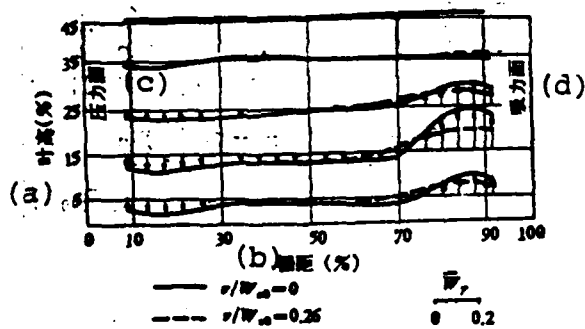Key: (a) Blade height (%); (b) Cascade spacing (%).

Fig. 2 Component velocity distribution in
the blade height direction.

Key: (a) Blade height (%); (b) Cascade spacing (%);
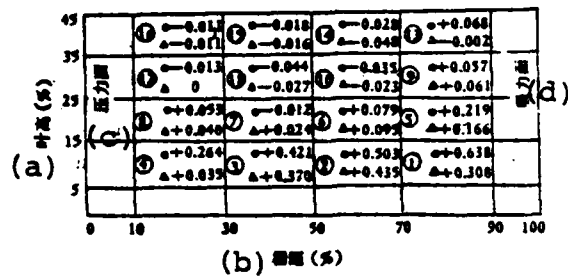(c) Pressure surface; (d) Suction surface.

Fig. 3 Distribution of vortex strength.
Key: (a) Blade height (%); (b) Cascade spacing(%);
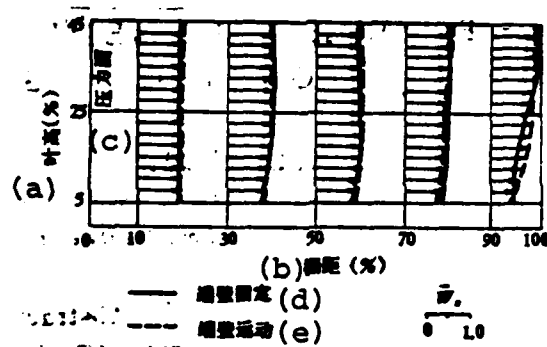(c) Pressure surface: (d) Suction surface.

Fig. 4 Distribution of main flow velocity.
Key: (a) Blade height (%); (b) Cascade spacing (%);
(c) Pressure surface; (d) End wall fixed;
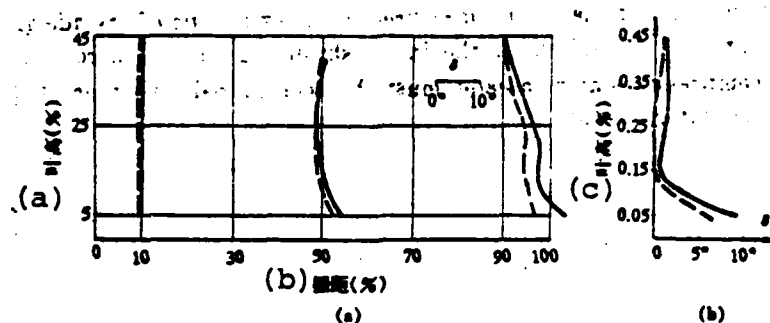(e) End wall moving.

28

Fig. 5 Distribution of air flow over-deflection angles.

Key: (a) Blade height (%); (b) Cascade spacing (%);
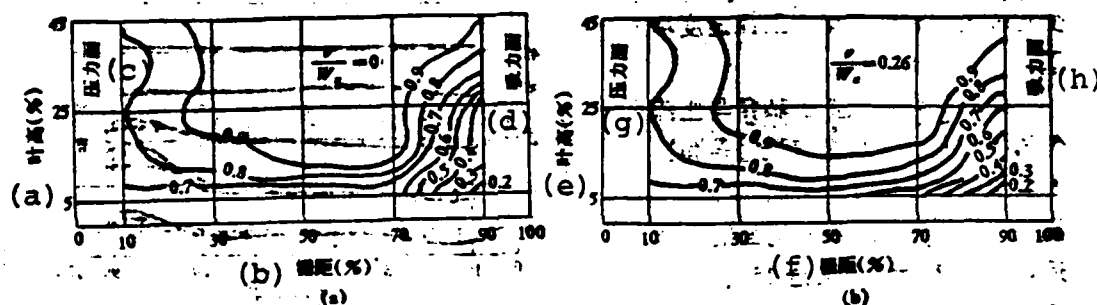   (c) Blade height (%).

Fig. 6 Total pressure isobars of tip region.

Key: (a) Blade height (%); (b) Cascade spacing (%);
     (c) Pressure surface; (d) Suction surface;
     (e) Blade height (%); (f) Cascade spacing (%);
     (g) Pressure surface; (h) Suction surface.

References

[1] Horlock, J.H., Lakshminarayan, B.: Secondary Flows Theory.
    Experiment and Application in Turbomachinery Aerodynamics,
    Annual Review of Fluid Mechanics, 5 (1973), 247.

[2] Cai Ruixian, Wang Xigang, Peng Huijun and Wu Bujing: The
    effect of stator blade inner shrouding on aerodynamic
    properties of axial flow compressors and the thermodynamic
    properties of a 4500HP locomotive gas turbine, Journal of
    Engineering Thermophysics, I, 1, (1980), 1.

[3] Jefferson, J.L., Turner, R.C.: Some Shrouding and Tip
    Clearing Effects in Axial Flow Compressor, I.S.P., 5,
    (1958), 42.

[4] Langston, L.S.: Crossflows in a Turbine Cascade Passage,
    Journal of Engineering for Power, 4, (1980), 866.

DATA CORRELATION FOR THE EFFECTIVE FLOW RANGE OF COMPRESSOR
CASCADES

Guo Jinghua, Qi Lianzhong and Zhang Chunlin
Marine Boiler and Turbine Research Institute

Abstract

This paper presents a semi-analytical method for
calculating the compressor cascade throat width and the
correlation of effective inlet flow angle range with
critical mach number is given. Good agreement between
the prediction and test results is observed.

I. INTRODUCTION

Reference 1 summarizes the test results of a circular arc
mean camber line C_4 series cascade and proposes a method of data
correlation of the inlet flow angle which changes with the Mach
number and is determined by the principle of twice the minimum
loss. A suitable design for the angle of attack is chosen by
using the cascade curve $a_1 \sim M_{NC}$ so as to guarantee the high
efficiency of the design. At the same time it ensures that
there is adequate stall and blocking allowance in the off-design
operation. These design requirements can be satisfied by changing
the curve $a_1 \sim M_{NC}$ through modifying the cross section geometry
of the blade row.

When modifying the compressor, the curve $a_1 \sim M_{NC}$ can be
used to analyze the operating conditions of the blade row cross
section so as to determine the location of a breakdown or of a
basic level of inferior performance. A program of rematching is
proposed and also of doing quantitative estimates. It is there-
fore a powerful tool in guiding compressor design and modifica-
tion. It is of immense practical value to apply this method of
correlation to our commonly used A_{40} compressor profile.

II. CORRELATION METHOD

The correlation method is basically the same as in reference 1, except some of the correlation curves have been redrawn on the basis of data in reference 2 and others have been corrected in accordance with the difference between two types of profiles (the mean camber line shape and the equal leading edge thickness).

1. Relative Throat Width of Cascade o/s

In order to raise accuracy, the method in reference 1 was not used. A semi-analytical method of calculation has been used (see fig. 1).

The equation for a parabolic mean camber line with the maximum curvature at 45% of chord length is:

$$1/\bar{y} = ctg\kappa_1/\bar{z} + ctg\kappa_2/(1-\bar{z});$$

The back arc coordinate $(\bar{x}'_i, \bar{y}'_i)$ can be found by the following formula:

$$\bar{x}_i = \bar{x}_i - \bar{y}_{li}\sin a_i; \quad \bar{y}_i = \bar{y}_i + \bar{y}_{li}\cos a_i$$

In the formula, $\bar{y}_{li}$ is the half thickness of the profile and a_i can be found by the differential of the mean camber line equation.

$$a_i = arctg\{\bar{y}_i^2[ctg\kappa_1/\bar{z}_i^2 - ctg\kappa_2/(1-\bar{z}_i)^2]\}$$

In this way, the problem of finding o/s can be summed up as finding the minimum distance $(o/c)_{min}$ from the leading edge center of the adjacent blade $M(\bar{x}_m, \bar{y}_m)$ to the back arc.

Finally, o/s$= [(o/c)_{min} - r/c]/(s/c)$; where r is the radius of the leading edge of the profile.

32

2. Maximum Critical Mach Number M_{NC}^H

The inlet angle range (or angle of attack range) determined by twice the minimum loss drops with an increase in the Mach number. When this range tends to be zero, the relative critical Mach number is known as the maximum critical Mach number. It mainly depends on the curvature of airflow inside the blades and on blade spacing. By using the data in reference 2 the curve $a_1 \sim M_{NC}$ can be made, M_{NC}^H can be obtained and with the correlation of the relative blade angle of curvature θ and nodal chord ratio s/c, the curve $M_{NC}^H / \psi_1 \; \psi_2 \sim \theta \cdot$ s/c can be obtained as in fig. 2.

In the figure, ψ_1, ψ_2 are the correction factors taking into consideration the effect of relative blade thickness t/c (t/c=0.1 is a basic reference value) and the inlet blade angle a_1' (a_1'=45° is a basic reference value) on M_{NC}^H. The correction curves can be expressed by the following polynomials:

$$\phi_1 = 1.03943 + 1.10357(t/c) - 14.6429(t/c)^2$$
$$\phi_2 = 0.931 + 0.00157 \cdot a_1'$$

3. Optimal Inlet Angle a_1^H

The corresponding minimum loss inlet angle relative to the maximum critical Mach number is called the optimal inlet angle. For a profile with the same thickness, a_1^H depends on o/s. By using the data in reference 2, it is also possible to establish the relational curve in fig. 3.

4. Positive and Negative Stall Angle of Attack Change in Relation to Mach Number

The relational curve between the change in the positive stall allowance $(a_1 - a_1^H)/x_1 \cdot x_2$ and negative stall allowance

(cos a_1 - cos a_1^H)/Ω and (M_{NC}^H - M_{NC}) is given in reference 1.
Figure 4 uses data from reference 2 to obtain two relational curves.

In the figure, x_1 takes into consideration the effect of blade thickness. Because the relative distance between the thickness of the profiles A_{40} and C_4 is extremely small, the coefficient x_1 is considered to be identical with C_4. x_2 takes into consideration the effect of the nodal chord ratio and angle of curvature on the allowance for positive stall. By using θ=25°, s/c=1.0 as a basic reference value, the curve for x_2 is made (fig. 5). Ω takes into consideration the effect of s/c and a_1' on the allowance for negative stall (fig. 6).

III. CALCULATION RESULTS

On the basis of the correlation method introduced in this paper, the $a_1 \sim M_{NC}$ curves for 14 cascades from reference 2 were calculated. These tallied well with the predicted results. Using numbers 4 and 5 cascades as examples: the difference between the $a_1 \sim M_{NC}$ curves obtained using the calculation method in reference 1 and the tests was relatively large; after using the method in this paper to determine o/s, the method in reference 1 was used. Although there was some improvement of the difference between the experiment and the a_1^H, M_{NC}^H, the positive and negative stall boundaries of the effective flow range could still be observed as different from the experiment. The third type clearly tallies well with the method in this paper (see fig. 7).
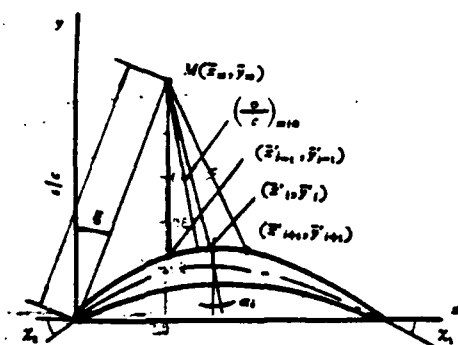
Fig. 1 Diagram for determining relative
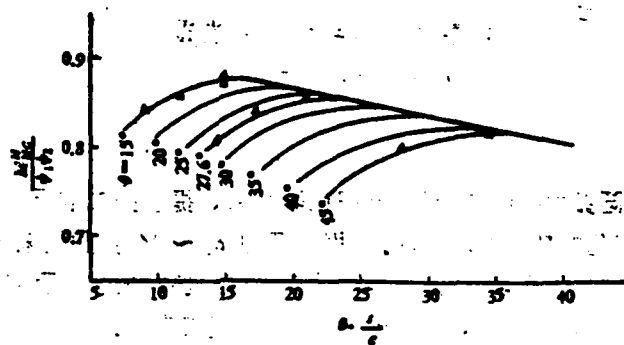throat width.

Fig. 2 Relational curve of maximum
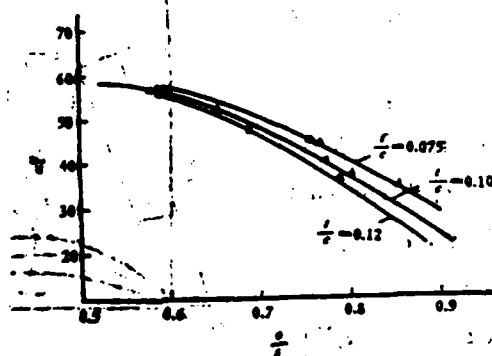critical Mach number on curvature
and nodal chord ratio.

Fig. 3 Relational curve of optimal inlet
angle on relative throat width.

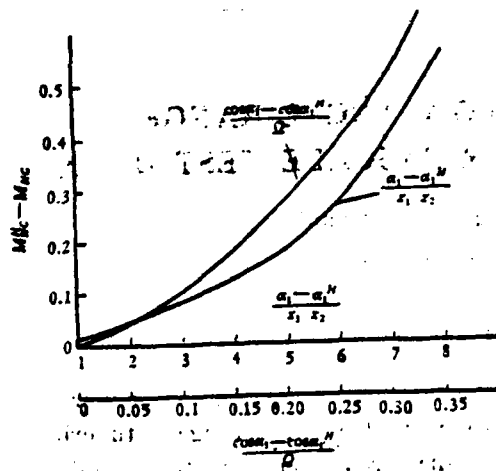35

Fig. 4 Curve showing $\dfrac{a_1-a_1^H}{x_1 x_2}$ and $\dfrac{\cos a_1-\cos a_1^H}{\Omega}$
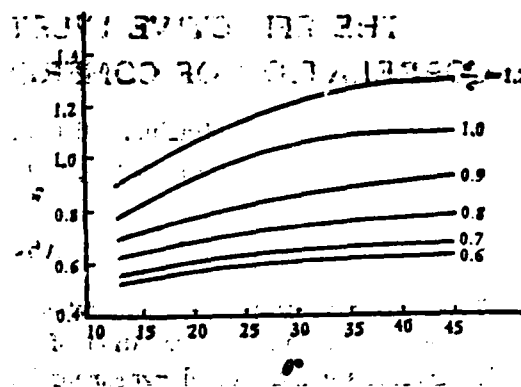
changes with $(M_{NC}^H - M_{NC})$.

Fig. 5 Positive stall boundary correction factors.
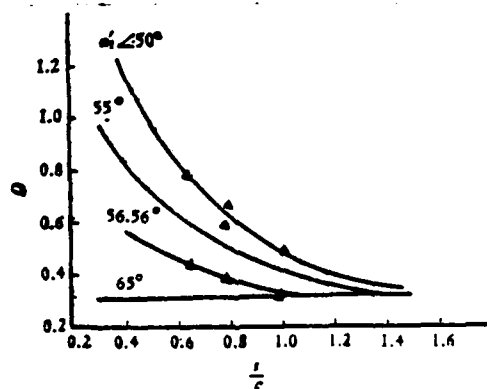
Fig. 6 Negative stall boundary correction factors.

36
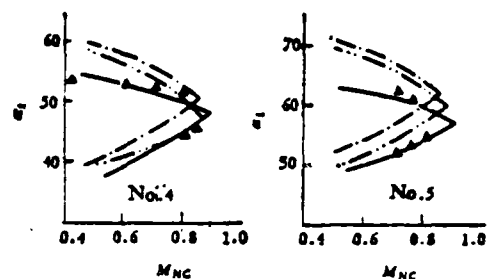
(a) ---[1]的方法
(b) -·-·-确定 o/s 后,仍用[1]的方法
(c) 一本文的方法
(d) ▲ 文献[2]中的 No.5、No.6 叶栅吹风数据

Fig. 7   Comparison of calculation results
          with test.

Key: (a) Method of reference 1; (b) Reference
     1 method still used after determining
     o/s; (c) Our method; (d) Test data for
     nos. 5 and 6 cascades in reference 2.

References

[1] J.S. Coleman: Spey Mk 202 Compressors Aerodynamic Supporting
    Cascade Data, RCR, 12054, 1976.

[2] A.I. Bunimorich, G.S. Orlova: Symposium of Aerodynamic
    Characteristics of Flat Compressor Screens, MAP, USSR, 1951.

THE HODOGRAPH METHOD DESIGN FOR TRANSONIC TURBINE CASCADES ON SURFACES OF REVOLUTION

Chen Zuoyi

Qinghua University

Abstract

Applying the basic equation of hodograph method corresponding to the S_1 surface, the calculated methods and equations of hodograph design for transonic turbine cascade in revolutionary surface are presented, and on basis of the simplified condition, the solution for mixed type equation corresponding to the compressible function in revolutionary surface is derived, the calculated results of profiles are also presented.

Previous hodograph method design has been limited to plane flow. This paper is the first to propose velocity coordinate flow function equations corresponding to flow surfaces of revolution and integral equations returning from velocity surface to stream surface. These serve as the basic equations for the calculation of the subsonic region components of a transonic turbine cascade. In the supersonic region we started from the flow function equation of the velocity coordinate corresponding to the surface of revolution, and derived the compressibility function corresponding to the flow surface of revolution. Furthermore, we were able to apply mixed type equations to the surface of revolution.

I. FLOW FUNCTION EQUATIONS OF VELOCITY COORDINATES CORRESPONDING TO THE FLOW SURFACE OF REVOLUTION AND THEIR CALCULATION FORMULA

Applying the basic relationship of three dimensional flow to velocity potential and stream function and the basic principles of conversion between the velocity surface and the physical surface, we deduced the velocity coordinate stream function

equation corresponding to the surface of revolution, as follows:

$$\frac{\sqrt{\varepsilon}}{\bar{b}\bar{\rho}} M^* \frac{\partial^2\psi}{\partial M^{*2}} + \left[\frac{\sqrt{\varepsilon}}{\bar{b}\bar{\rho}} + \frac{\partial\left(\frac{\sqrt{\varepsilon}}{\bar{b}\bar{\rho}}\right)}{\partial M^*} M^* + \frac{\partial^2\left(\frac{\sqrt{\varepsilon}}{\bar{b}\bar{\rho}}\right)}{\partial\theta^2}\right] \frac{\partial\psi}{\partial M^*}$$

$$+ \frac{\partial\left(\frac{\sqrt{\varepsilon}}{\bar{b}\bar{\rho}}\right)}{\partial\theta} \frac{\partial^2\psi}{\partial M^*\partial\theta} + \left[\frac{1}{M^*}\frac{\partial\left(\frac{\sqrt{\varepsilon}}{\bar{b}\bar{\rho}}\right)}{\partial\theta} - \frac{\partial^2\left(\frac{\sqrt{\varepsilon}}{\bar{b}\bar{\rho}}\right)}{\partial M^*\partial\theta}\right] \frac{\partial\psi}{\partial\theta}$$

$$+ \left[\frac{1}{M^*}\frac{\sqrt{\varepsilon}}{\bar{b}\bar{\rho}} - \frac{\partial\left(\frac{\sqrt{\varepsilon}}{\bar{b}\bar{\rho}}\right)}{\partial M^*}\right] \frac{\partial^2\psi}{\partial\theta^2} = 0 \qquad (1)$$

In the equation, $\bar{b}=b/b_0$ and $\bar{\rho} = \rho/\rho*$ are both dimensionless quantities.

For the cone's surface of revolution, $\sqrt{\varepsilon}$ is a constant. By taking all the compound derivatives in (1) and developing and justifying them, and then inserting the regular stream function ψ_r, $L(\psi_r)=L(\psi)-L(\psi_\infty)$ is satisfied.

Therefore, in solving the equation of velocity coordinate stream function equation corresponding to the cone, it is only necessary to solve the partial differential equation of the following regular stream function:

$$M^*\phi_{r_{M^*M^*}} + \left[1 - \frac{M^*}{\bar{b}}\bar{b}_{M^*} - \frac{M^*}{\bar{\rho}}\bar{\rho}_{M^*} + \frac{2}{\bar{\rho}}\bar{b}_\theta - \frac{1}{\bar{\rho}}\bar{b}_{\theta\theta}\right]\phi_{r_{M^*}} - \frac{\bar{b}_\theta}{\bar{b}}\phi_{r_{M^*\theta}}$$

$$- \left[\frac{\bar{b}_\theta}{M^*\bar{b}} + \frac{2\bar{b}_{M^*}\bar{b}_\theta}{\bar{\rho}\bar{\rho}} + \frac{\bar{b}_\theta\bar{\rho}_{M^*}}{\bar{b}\bar{\rho}^2} + \frac{\bar{b}_{M^*\theta}}{\bar{b}}\right]\phi_{\theta\theta} + \left[\frac{1}{M^*} + \frac{\bar{b}_{M^*}}{\bar{b}}\right.$$

$$\left. + \frac{\bar{\rho}_{M^*}}{\bar{\rho}}\right]\phi_{r_{\theta\theta}} + L(\phi_\infty) = 0 \qquad (2)$$

. The relative thickness of the flow blade $\bar{b}$ is a function of M^*, θ. Its final determination depends on the whole hodograph

design of the three dimensional flow. To simplify the calculations in this paper, we used the linear relationship expression $\bar{b}=c_1 M^* + c_2\,\theta$, where c_1 and c_2 are constants. By inserting it in equation (4), the partial differential equation of the regular stream function used in actual calculation is obtained as follows:

$$M^*\phi_n \left[\cdots\right] - \frac{M^*}{\bar{b}}\rho_m + \frac{2}{\bar{b}}c_1^2\left[\phi_{r_m}\cdots\phi_m\cdots\right]_{M^*\bar{b}}^{c_1}$$
$$+ \frac{2c_1c_2}{\bar{b}\bar{\rho}} + \frac{c_2\rho_1 r^2}{\bar{b}\bar{\rho}^2}\right]\phi_{\theta} \pm \left[\frac{1}{M^*}+\frac{\sigma_1}{\bar{b}}\pm\frac{c\theta}{\bar{\rho}}\right]\phi_{r\theta} + L(\phi_{\infty}) = 0 \qquad (3)$$

In order to fit the requirements of the random boundary node, a random curve grid was used. If M*, θ is an orthogonal linear grid, m*, θ is a random curve grid and the included angle of M* and m* is a, then m* and θ are equations of regular stream functions expressed by variables as in:

$$M^*\left(\phi_{r_m \cdot_m}\cdot\frac{1}{\cos^2 a} + \phi_{\theta\theta}\,\mathrm{tg}^2 a + 2\phi_{r_m \cdot_\theta}\frac{\mathrm{tg}\,a}{\cos a}\right) + H_1\left(\phi_{r_m \cdot}\frac{1}{\cos a} + \phi_{r_\theta}\,\mathrm{tg}\,a\right)$$
$$- H_2\left(\phi_{r_m \cdot_\theta}\frac{1}{\cos a} + \phi_{r_\theta\theta}\,\mathrm{tg}\,a\right) - H_3\phi_{r_\theta} + H_4\phi_{r_{\theta\theta}} + L(\phi_{\infty}) = 0 \qquad (4)$$

In the equation, the coefficients H_1, H_2, H_3 and H_4 are all functions of M* and θ.

II. INTEGRAL EQUATION FOR RETURNING PHYSICAL STREAM SURFACE

After finding ψ_r by equation (4), ψ can be found on the basis of the relationship between ψ_r and ψ_{∞} . The profile coordinates can then be found by returning the physical surface by the distribution of ψ . If the initial radius opposite the cone stream surface is R_0 and the cone angle is a_1, then:

$$R = R_0 + Z\,\mathrm{tg}\,a$$

40

The coordinates of the surface of revolution are expressed by Z, φ, and R, since the relationship between R and Z on the cone has already been determined. For this reason, in finding the profile contour, the relationship between the two coordinates Z and φ is all that is required. Their integral equations are:

$$Z - Z_* = \int_{\theta_*}^{\theta} \frac{h\rho_\infty M_\infty^* \cos\theta_\infty \cos\theta}{M^* \rho^*}$$

$$\cdot \left[\frac{\partial\left(\frac{1}{\bar{\rho}\bar{b}}\right)}{\partial\theta} \frac{\partial\psi}{\partial\theta} + \frac{1}{\bar{b}\bar{\rho}M^*} \frac{\left(\frac{\partial\psi}{\partial\theta}\right)^2}{\frac{\partial\psi}{\partial M^*}} - \frac{\left(\frac{\partial\psi}{\partial\theta}\right)^2}{\frac{\partial\psi}{\partial M^*}} \frac{\partial\left(\frac{1}{\bar{b}\bar{\rho}}\right)}{\partial M^*} + \frac{M^*}{\bar{b}\bar{\rho}} \frac{\partial\psi}{\partial M^*} \right] d\theta \quad (5)$$

$$\varphi - \varphi_* = \int_{\theta_*}^{\theta} \frac{h\rho_\infty M_\infty^* \cos\theta_\infty \sin\theta}{(R_* + Z \operatorname{tg}\alpha_1)M^* \rho^*}$$

$$\cdot \left[\frac{\partial\left(\frac{1}{\bar{\rho}\bar{b}}\right)}{\partial\theta} \frac{\partial\psi}{\partial\theta} + \frac{1}{\bar{b}\bar{\rho}M^*} \frac{\left(\frac{\partial\psi}{\partial\theta}\right)^2}{\frac{\partial\psi}{\partial M^*}} - \frac{\left(\frac{\partial\psi}{\partial\theta}\right)^2}{\frac{\partial\psi}{\partial M^*}} \frac{\partial\left(\frac{1}{\bar{b}\bar{\rho}}\right)}{\partial M^*} + \frac{M^*}{\bar{b}\bar{\rho}} \frac{\partial\psi}{\partial M^*} \right] d\theta \quad (6)$$

III. THE MIXED TYPE EQUATION CORRESPONDING TO THE SURFACE OF VELOCITY ON THE CONE STREAM SURFACE AND ITS NOZZLE SOLUTION

Applying a nozzle solution to the supersonic components during design means there is little change in the contour θ of the turbine cascade and relatively large change in M*. If we suppose that $\bar{b} = c_1 M^*$, by substituting it in equation (1) and introducing the new variable $d\sigma = -K dM^*$, we get:

$$M^* \left[\psi_{\sigma\sigma} K^2 - \psi_\sigma \frac{dK}{d\sigma} \right] - \frac{M^*}{\bar{\rho}} \bar{\rho}_{M^*} [-K\psi_\sigma] + \left[\frac{2}{M^*} + \frac{\bar{\rho}_{M^*}}{\bar{\rho}} \right] \psi_{\theta\theta} = 0 \quad (7)$$

Clearly, if equation (7) can be given the mixed type equation $K(\sigma)\psi_{\theta\theta} + \psi_{\sigma\sigma} = 0$ of the plane flow by making the coefficient of ψ_σ zero, then to satisfy $M^* \frac{dK}{d\sigma} - \frac{M^*}{\bar{\rho}} \bar{\rho}_{M^*} K$ K must be

$$-K = e^{\int \frac{\bar{\rho}_{M^*}}{\bar{\rho}} dM^*} \quad (8)$$

41

Equation (7) then changes to:

$$F(\sigma)\psi_{\theta\theta} + \psi_{\sigma\sigma} = 0 \qquad (9)$$

In the equation

$$F(\sigma) = \left[\frac{2}{M^*} - \frac{\beta M^*}{\bar{\rho}}\right] / (M^* K^2)$$

F(σ) is the compressibility function of the mixed type equation corresponding to the surface of velocity of the cone.

If the expanded Tricomi approximate solution is used in the design, only if we can find an approximate function will it have the form of an expanded Tricomi compressibility function and be near enough to F(σ) in numerical value. If the approximate function $F_a(\sigma) = \frac{B^6 \sigma}{(1-Cb\sigma)^5}$, we can use the two following boundary conditions to determine the coefficients B and C:

1.　　　$\left[\frac{dF_a(\sigma)}{d\sigma}\right]_{M^*=1} = \left[\frac{dF(\sigma)}{d\sigma}\right]_{M^*=1}$ 　　　(10)

2.　　　$[F_a(\sigma)]_{M^*=1} = [F(\sigma)]_{M^*=1}$ 　　　(11)

Furthermore, the coefficients C and B of the approximate compressibility function are obtained.

Figure 1 shows the profile of a hodograph method design carried out on a cone. The design parameters are: r=1.29, M_∞ =0.238, θ_∞ =0, T_∞ =1490K, θ_{out}=73°, M^*_{out}=1.15, R_0=300mm, a_1=26.56°, H_0=50.05mm. From the calculations we can know that the difference in laws of velocity distribution and similar parameters is extremely large on cones and on planes. Therefore, the effect of three dimensions must be considered in transonic cascade design.
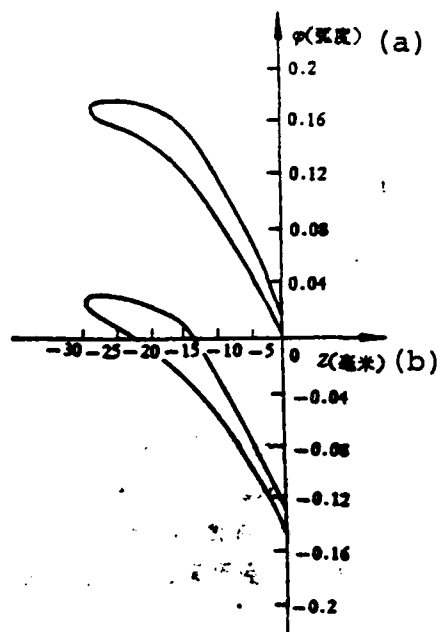
42

Fig. 1 Hodograph method design for transonic
turbine profile on a cone.

Key: (a) Radian; (b) Millimeters.

BASIC AERODYNAMIC EQUATIONS EXPRESSED BY PARTIAL DERIVATIVES ALONG AN ARBITRARY STREAM SURFACE IN SEMI-ORTHOGONAL CURVILINEAR COORDINATE SYSTEMS

Wang Zhongqi

Harbin Institute of Technology

Abstract

Basic aerodynamic equations expressed by partial derivatives along an arbitrary stream surface in semi-orthogonal curvilinear coordinate system have been derived in this paper. These equations are applicable not only to relative stream surfaces S_1 (when $\sqrt{g_{33}}=1$) but also to S_2 (when $\sqrt{g_{33}}=r$). They are also suitable for cylindrical coordinate system, if $x^3=1$, $x^2=-\varphi$ and $x^1=z$.

I. BASIC AEROTHERMODYNAMIC EQUATIONS

We used a semi-orthogonal curvilinear coordinate system of corresponding unit base vectors and by using formulas (11) - (17) in reference 1 we were able to express the vector form of the basic equation of aerodynamics as the scalar quantity form in a curvilinear coordinate system.

1. Equation of continuity

$$\frac{\partial\left(\sqrt{g/g_{11}}\,\rho W^1\right)}{\partial x^1}+\frac{\partial\left(\sqrt{g/g_{22}}\,\rho W^2\right)}{\partial x^2}+\frac{\partial\left(\sqrt{g/g_{33}}\,\rho W^3\right)}{\partial x^3}=0 \qquad (1)$$

2. Equation of motion

$$\frac{W^\beta}{\sqrt{g_{\beta\beta}}}\left[\frac{\partial\left(\sqrt{g_{\beta\beta}}\,W_\beta\right)}{\partial x^\alpha}-\frac{\partial\left(\sqrt{g_{\alpha\alpha}}\,W_\alpha\right)}{\partial x^\beta}\right]+2\frac{W^\beta}{\sqrt{g_{\beta\beta}}}\sqrt{\frac{g}{g_{\tau\tau}}}\,\Omega^\tau$$

$$-\frac{W^\tau}{\sqrt{g_{\tau\tau}}}\left[\frac{\partial\left(\sqrt{g_{\alpha\alpha}}\,W_\alpha\right)}{\partial x^\tau}-\frac{\partial\left(\sqrt{g_{\tau\tau}}\,W_\tau\right)}{\partial x^\alpha}\right]-2\frac{W^\tau}{\sqrt{g_{\tau\tau}}}\sqrt{\frac{g}{g_{\beta\beta}}}\,\Omega^\beta$$

$$=\frac{\partial I}{\partial x^\alpha}-T\frac{\partial s}{\partial x^\alpha} \qquad (2)$$

In the equation, the corner symbols α, β and γ are

44

assigned values according to the "cyclic law." Therefore, equation (4) separately expresses a partial equation of motion along the direction of three curvilinear coordinates. Ω^a (a=1,2,3) expresses the inverse variant physical component of the angular velocity vector ω of turbo-machinery revolutions. By using the triangles och, oab and ofd in fig. 1, it is not difficult to obtain:

$$\Omega^1 = \omega(\cos\xi\cos\eta + \sin\xi\cos\theta_{13}\cos^2\eta/S) \tag{3}$$

$$\Omega^2 = -\omega\sin\xi/S \tag{4}$$

$$\Omega^3 = -\omega(\cos\xi + \sin\xi\cos\eta\cos\theta_{12}/S)\sin\eta \tag{5}$$

In the formulas, $S = \sqrt{1 - \cos^2\eta\cos^2\theta_{12}}$

3. Equation of energy

$$\frac{W^1}{\sqrt{g_{11}}}\frac{\partial I}{\partial x^1} + \frac{W^2}{\sqrt{g_{22}}}\frac{\partial I}{\partial x^2} + \frac{W^3}{\sqrt{g_{33}}}\frac{\partial I}{\partial x^3} = 0 \tag{6}$$

II. BASIC AERODYNAMIC EQUATION ALONG A STREAM SURFACE

The relationship between the partial derivative of parameter q along the stream surface and the ordinary partial derivative can be expressed as

$$\frac{\delta q}{\delta x^1} = \frac{\partial q}{\partial x^1} - \frac{N_1\sqrt{g_{11}}}{N_3\sqrt{g_{33}}}\frac{\partial q}{\partial x^3}, \quad \frac{\delta q}{\delta x^2} = \frac{\partial q}{\partial x^2} - \frac{N_2\sqrt{g_{22}}}{N_3\sqrt{g_{33}}}\frac{\partial q}{\partial x^3} \tag{7}$$

By using this expression, the basic aerodynamic equation expressed by a partial derivative along the stream surface is obtained from equations (1), (2) and (3) respectively.

1. Equation of continuity

$$\frac{\delta(\sqrt{g}g_{11}\rho W^1)}{\delta x^1} + \frac{\delta(\sqrt{g}/g_{22}t(\rho^2))}{\delta x^2} = 0 \qquad (8)$$

When x^3=const is separated into surface of revolution ($\sqrt{g_{33}}$=1) and meridian surface ($\sqrt{g_{33}}$=r), equation (8) correspondingly changes into

$$\frac{\delta(\sqrt{g_{22}}\sin\theta_{12}r\rho W^1)}{\delta x^1} + \frac{\delta(\sqrt{g_{11}}\sin\theta_{12}r\rho W^2)}{\delta x^2} = 0 \qquad (9)$$

$$\frac{\delta(\sqrt{g_{22}}\sin\theta_{12}rr\rho W^1)}{\delta x^1} + \frac{\delta(\sqrt{g_{11}}\sin\theta_{12}rr\rho W^2)}{\delta x^2} = 0 \qquad (10)$$

These two equations separately express the equations of continuity applied to stream surfaces S_1 and S_2, i.e. equations (43) and (43)* in reference 2.

2. Equation of motion

$$\frac{W^\beta}{\sqrt{g_{\beta\beta}}}\left[\frac{\delta(\sqrt{g_{\beta\beta}}W_\beta)}{\delta x^\alpha} - \frac{\delta(\sqrt{g_{\alpha\alpha}}W_\alpha)}{\delta x^\beta}\right] + \frac{W^3}{\sqrt{g_{33}}}\frac{\delta(\sqrt{g_{33}}W^3)}{\delta x^\alpha}$$
$$+ 2\sqrt{g_{\alpha\alpha}}\sin\theta_{12}(W^\beta\Omega^\gamma - W^\gamma\Omega^\beta) = \frac{\delta I}{\delta x^\alpha} - T\frac{\delta_s}{\delta x^\alpha} + f_\alpha^* \qquad (11)$$

In the formula

$$f_\alpha^* = \frac{N_\alpha\sqrt{g_{\alpha\alpha}}}{N_3\sqrt{g_{33}}}\left[\frac{1}{\rho}\frac{\partial p}{\partial x^3} - (\omega)^2 r\frac{\partial r}{\partial x^3} - W^1 W_2\frac{\partial\cos\theta_{12}}{\partial x^3} - \sum_{i=1}^{3}\frac{W^i W_i}{\sqrt{g_{ii}}}\frac{\partial\sqrt{g_{ii}}}{\partial x^3}\right] \qquad (12)$$

In these two equations, a , β and γ are assigned values according to the "cyclic law." It can be proved, in the three partial equations of motion along the stream surface, that only two are independent. Therefore, in the two above expressions, a can only have the two values of 1 and 2 and similarly, β and γ can only have two values. The partial equations of motion

46

along the stream surface in the x^1 and x^2 directions can now be obtained from equation (11). Furthermore, from equation (12) it can be seen that f_a^* includes two components; one component is related to the changes in force in the x^3 direction (changes in pressure and centrifugal inertial force) and the other is related to changes in the parameters O_{12}, g_{11}, g_{22} and g_{33} in the x^3 direction of the curvilinear coordinate system. It can be proved that, if $f_a^*(a=1,2,3)$ is taken as three covariant components of a vector f^*, then $f^* \perp W$.

3. Equation of energy

$$\frac{W^1}{\sqrt{g_{11}}}\frac{\partial I}{\partial x^1} + \frac{W^2}{\sqrt{g_{22}}}\frac{\partial I}{\partial x^2} = 0 \qquad (13)$$

It can be seen from this that there is no change in the form of the equation of energy, whether in coordinate surface x^3=constant which is a surface of revolution or in two classes of semi-orthogonal curvilinear coordinate systems of a meridian surface.

III. SEVERAL SPECIAL CONDITIONS OF PARTIAL EQUATIONS OF MOTION

1. When coordinate surface x^3=const is an arbitrary surface of revolution ($\sqrt{g_{33}}$=1), equation (11) is simplified into two partial equations of motion (a=1,2) expressed by partial derivatives along the stream surface S_1.

$$\frac{W^b}{\sqrt{g_{bb}}}\left[\frac{\partial(\sqrt{g_{bb}}W_b)}{\partial x^a} - \frac{\partial(\sqrt{g_{aa}}W_a)}{\partial x^b}\right] + W^3\frac{\partial W_3}{\partial x^a} + 2\sqrt{g_{aa}}\sin\theta_{12}(W^b\Omega^r - W^r\Omega^b)$$

$$= \frac{\partial I}{\partial x^a} - T\frac{\partial s}{\partial x^a} - f_a^* \qquad (14)$$

2. When coordinate surface x^3=const is an arbitrary surface of revolution and is also a stream surface, $W^3=W_3=0$, $f_1^*=f_2^*=0$ and equation (14) is simplified into equation (47) in reference 2. It can be proved that the two equations given in (14)

47

(corresponding to a=1,2) are identical.

3. When coordinate surface x^3=const is a cylindrical surface (x^3=r=const) and x^1=z, x^2= $-\varphi$, we obtain

$$\theta_{12} = 90°, \ \sqrt{g_{11}} = 1, \ \sqrt{g_{22}} = r, \ W^1 = W_1 = W_z, \ W^2 = W_2 = -W_\varphi,$$
$$W^3 = W_3 = W_r, \ N_1 = n_z, \ N_2 = -n_\varphi, \ N_3 = n_r, \ \Omega^3 = 0$$

Under these conditions, equation (14) is simplified into equation (39) in reference 3.

4. When coordinate surface x^3=const is a meridian surface, we obtain $\sqrt{g_{33}}$=r, x^3= φ , Ω^3=0, W^3=W_3=W_φ , $\angle \eta$ =0, $\angle \xi$ = $\angle \theta_1$, and by using formulas (3) and (4) we can obtain equation (92) in reference 2 from equation (11). From these conditions $\partial r/\partial \varphi = \partial \cos \theta_{12}/\partial \varphi = \partial \sqrt{g_{11}}/\partial \varphi = \partial \sqrt{g_{22}}/\partial \varphi = 0$, and equation (12) changes into equation (93) in reference 2.
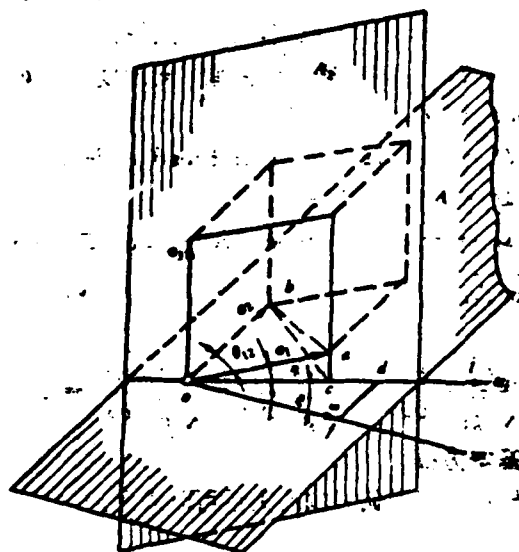

Fig. 1   The deduced inverse variant physical component Ω^a expression of angular velocity ω is used to chart the e_1 and e_3 coplane, and the ω and e_2 coplane.

48

References

[1] Wang Zhongqi, Lai Shengkai, Xu Wenyuan: Aerodynamic Calculation of Turbine Stator Cascades with Curvilinear Leaned Blades and Some Experimental Results, Symposium Papers, 5th ISABE. Bangalore, India, (1981).

[2] Wu Zhonghua: A Basic Equation for a Turbomechanical Three-Dimensional Flow of a Non-Orthogonal Curvilinear Coordinate and a Non-Orthogonal Velocity Component and its Solution, Journal of Mechanical Engineering, 15,1, (1979).

[3] Wu Zhonghua: A General Theory of Three-Dimensional Flow in Subsonic and Supersonic Turbomachines of Axial, Radial and Mixed Flow Types, NACA TN2604, (1952).

[4] A.P. Borisenko and N.E. Tarapov: Vector Analysis and Basic Tensor Calcualtion, 'Visshaya School', Moscow, 1963.

MEASUREMENT OF AERODYNAMIC PARAMETERS BEHIND ROTORS[*]

Liu Sihong

Northwestern Polytechnical University

Abstract

This paper analyzes and discusses the measurement errors which occur when measuring the total temperature and total pressure behind rotors. Focus is placed on solving the following problems: 1. The error equations of rotation state are derived by sweep integration for the first order system to square wave. It provides a relatively clear theoretical outline for the measurement errors behind rotors and the method and equations to calculate the errors of rotation state. 2. The mechanism of aerodynamic blockage and a new definition of aerodynamic ratio are briefly presented. An experimental curve of the blockage errors behind rotors and the ratio of aerodynamic blockage is given. 3. The method to decrease the measurement errors behind rotors is explored.

I. MEASUREMENT ERRORS BEHIND ROTORS

The aerodynamic parameters of total temperature and total pressure are measured behind rotors by a probe. Because of the rotation of the rotors, it is possible on the one hand to have the probe measure the mean operating parameters on the corresponding flux under conditions of non-circular motion. On the other hand, there can also be errors in measurement on account of the rotation. These types of errors are sometimes positive, sometimes negative, sometimes large and sometimes small. They cause scattering in the measured values and result in distortion. We analyze the tot l temperature as an example below.

1. Rotation State Errors

In turbine performance experiments it is the mean parameters of the ring surfaces and the whole outlet cross section which need to be determined. In order to obtain the mean total

---

temperature of the rotor outlet, the cascade spacing t_L must be based on the mass mean

$$T_m^* = \int_0^{t_L} T^* C_{2A} \rho \, dx \Big/ \int_0^{t_L} C_{2A} \rho \, dx \qquad (1)$$

If it is incompressible and ρ =const, then

$$T_m^* = \int_0^{t_L} T^* C_{2A} \, dx \Big/ \int_0^{t_L} C_{2A} \, dx \qquad (2)$$

In order to transform the space field into a time field, on the basis of circumferential velocity, u=const, x=ut, dt=dx/u replacement is carried out on equation (2), and we obtain

$$T_m^* = \int_0^{t_i} T^* C_{2A} \, dt \Big/ \int_0^{t_i} C_{2A} \, dt \qquad (3)$$

However, the thermocouple behind the rotor can only be affected by time mean values.

$$T_B^* = \int_0^{t_i} T^* \, dt / t_i \qquad (4)$$

Because the mass mean requires an axial velocity C_{2A} weighted mean, and the thermocouple a real time mean, that is an isobaric mean, along with the T_m^* error value, it is an error introduced with unsuitable weighting called the weighted error. It is expressed by $\Delta T_{weighted}$.

$$\Delta T_{weighted}^{(1)} = \int_0^{t_i} T^* \, dt / t_i - \int_0^{t_i} T^* C_{2A} \, dt \Big/ \int_0^{t_i} C_{2A} \, dt \qquad (5)$$

Key: (1) Weighted.

When the rotor sweeps past the thermocouple at high speeds, the temperature T_j measured at the thermocouple contact point cannot keep up with changes in the total temperature of the airflow because of the thermal inertia of the thermocouple. Therefore, the thermocouple can only give time mean values of T_j.

These types of errors introduced because of inertia are known as dynamic response erros and are expressed by $\Delta T_{response}$.

(1)

$$\Delta T_{\text{响}} = \left[\int_0^{t_i} T_i^* dt - \int_0^{t_i} T^* dt\right]\Big/ t_i \qquad (7)$$

Key: (1) Response.

Weighted errors and dynamic response errors are caused by the rotor being in the rotation state. Hence, they are both known as rotation state errors and are expressed by $\Delta T_{rotation}$.

(1)   (2)   (3)

$$\Delta T_{\text{转}} = T_{Hj} - T_m^* = \Delta T_{\text{权}} + \Delta T_{\text{响}} \qquad (8)$$

Key: (1) Rotation; (2) Weighted; (3) Response.

There can also be these types of errors in the measurement of total pressure behind the rotor.

(1)

$$\Delta P_{\text{权}} = \int_0^{t_i} P^* dt / t_i - \int_0^{t_i} P^* C_{2A} dt \Big/ \int_0^{t_i} C_{2A} dt \qquad (9)$$

(2)

$$\Delta P_{\text{响}} = \left[\int_0^{t_i} P_i dt - \int_0^{t_i} P^* dt\right]\Big/ t_i \qquad (10)$$

(3)

$$\Delta P_{\text{转}} = P_{Hj} - P_m^* = \Delta P_{\text{权}} + \Delta P_{\text{响}} \qquad (11)$$

(4)   (5)

Key: (1) Weighted; (2) Response; (3) Rotation;
(4) Weighted; (5) Response.

2. Aerodynamic Blockage Errors

The probe located downstream of the rotor can increase the corresponding back pressure of the channel outlet and produce aerodynamic blockage. Aerodynamic blockage is not only determined by the ratio of the windward area of the probe and the channel outlet f/F_b, but is also related to the characteristic measurement d of the blockage matter and its distance l from the

channel outlet. For this reason, if the aerodynamic blockage is only measured in area ratio as is done for geometric blockage, the results will not be satisfactory. Here, $fd/F_{bl}\%$ is defined as the aerodynamic blockage ratio and it is used to indicate the level of aerodynamic blockage. Figure 1 shows the experimental curve of relative blockage errors behind the double stage turbine of a turbojet which change with the aerodynamic blockage ratio. The results show that the blockage causes the measured value of temperature T_4^* behind the turbine to be on the high side. When the aerodynamic blockage ratio reaches 16.5%, it corresponds to the blockage error of the maximum state M and the rated state H, a turbine temperature of 2.7% and 2.9% of ΔT_T respectively. With the rearward shift of the probe and after the aerodynamic blockage ratio has dropped to 6%, $\Delta T_4^*/\Delta T_T\% < 0.25\%$.
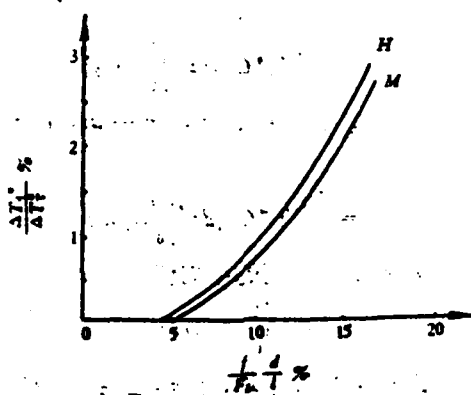

Fig. 1.

II. THE ANALYTICAL ANALYSIS OF ROTATION STATE ERRORS

The flow fields behind each channel of the rotor are not completely identical, however an equivalent mean characteristic can always be used as a substitute. Consequently, rotation state

53

errors can be obtained from an analysis of the measured values behind this channel. In view of the fact that temperature and pressure signals along the cascade spacing are frequently not continuous, sweep integration is used here to derive the rotation state error equation. So-called sweep integration consists of first dividing the cascade spacing into several subintervals and making each subinterval satisfy the requirements of continuity. Afterwards, there is successive sweeping beginning at the first subinterval. The probe is then placed at the final value of the preceding subinterval, that is, it enters this subinterval as an intitial value, and there is one by one integration.

For the purpose of conciseness, a flow field behind the rotor approximating a rectangular wave fitting was used (fig. 2) and given the probe is a first order system, rotation state errors of total temperature and total pressure are respectively discussed under conditions where the trail relative thickness $\bar{b}$ is both relatively thick and relatively thin.

For fig. 3a, the condition is shown where $\bar{b}$ is relatively thin and the choice of the coordinate can be divided into the two subintervals $0 \sim t_b$ and $t_b \sim t_s$. Each subinterval is a step. The step quantity for the total temperature is $D=T^*-T_{j0}$. Because the transfer function of a one order system is $G(s)=1/(1+\mathcal{T}s)$, therefore

$$L[T_j - T_m] = L[D]/G(s)$$

The thermocouple's temperature can be obtained according to the Laplace inverse transform,

$$T_j = T_m + (T_j^* - T_m)(1 - e^{-t/\tau}) \qquad (12)$$

We substitute formula (12) into formula (6) and integrate according to the following conditions

$0 < t < t_b,\ T^* = T_b^*,\ C_{2d} = C_{2dT}\ T_A = \dots$

$t_b < t < t_d,\ T^* = T_d^*,\ C_{2d} = C_{2b}\ T_B = T_{bi} = T_b^* + (T_b^* - T_d^*)(L - e^{-t/\tau}).$

and let

$$\bar{a} = t_a/t,\ \bar{c}_{2d} = a/\tau_L,\ \bar{b} = t_b/t,\ \bar{c} = b/t_L.$$

$$T_{Hi}^* = \bar{b}T_b^* + \bar{a}T_d^* + \frac{\tau}{t_s}(T_b^* - T_d^*)(1 - e^{-t/\tau})[(e^{-t/\tau} + e^{-t/\tau}) - 1]\quad (13)$$

Further, from formula (13), we obtain

$$T_m^* = (T_b^* \bar{b} C_{2b} + T_d^* \bar{a} C_{2d})/(\bar{a}C_{2b} + \bar{b}C_{2d})\quad (14)$$

The equation of rotation state errors is then obtained by substituting formulas (13) and (14) into formula (8)

$$\Delta T_R = \bar{a}(1 - \bar{a})(T_b^* - T_d^*)(C_{2b} - C_{2b})/(\bar{a}C_{2b} + \bar{b}C_{2b})$$

(1)

$$+ \frac{\tau}{t}(T_b^* - T_d^*)(1 - e^{-t/\tau})[(e^{-t/\tau} - e^{-t/\tau}) - 1]\quad (15)$$

Key: (1) Rotation.

For the same reason, when $\bar{b}$ is relatively thin, the equation of the rotation state error of total pressure is:

(1)

$$\Delta P_R = \bar{a}(1 - \bar{a})(P_b^* - P_d^*)(C_{2b} - C_{2b})/(\bar{a}C_{2b} + \bar{b}C_{2b})$$

$$+ \frac{\tau_2}{t_s}(P_b^* - P_d^*)(1 - e^{-t/\tau})[(e^{-t/\tau} - e^{-t/\tau}) - 1]\quad (16)$$

Key: (1) Rotation.

When $\bar{b}$ is relatively thick (fig. 3b), the respective equations for the rotation state errors of total temperature and total pressure are:

(1)

$$\Delta T_R = \bar{a}(1 - \bar{a})(T_b^* - T_d^*)(C_{2b} - C_{2b})/(\bar{a}C_{2b} + \bar{b}C_{2b})$$

$$+ \frac{\tau}{t_s}(T_b^* - T_d^*)(1 - e^{-t/\tau})[1 - (e^{-t/\tau} - e^{-t/\tau})]\quad (17)$$

$$\Delta P_R = \bar{a}(1 - \bar{a})(P_b^* - P_d^*)(C_{2b} - C_{2b})/(\bar{a}C_{2b} + \bar{b}C_{2b})$$

(2)

$$+ \frac{\tau_2}{t_s}(P_b^* - P_d^*)(1 - e^{-t/\tau})[1 - (e^{-t/\tau} - e^{-t/\tau})]\quad (18)$$

Key: (1) Rotation; (2) Rotation.

55

For the condition shown in fig. 3, we know from equations (5) and (9) that the respective equations for weighted errors of total temperature and total pressure are:

$$\Delta \overset{(1)}{T_\mathscr{E}} = \bar{a}(1-\bar{a})(T_b^* - T_a^*)(\overline{C_{2a} - C_{2b}})/(\bar{a}C_{2r} + \bar{b}C_{2b}) \qquad (19)$$

$$\Delta \overset{}{\overline{P_\mathscr{E}}} = \bar{a}(1-\bar{a})(P_b^* - P_a^*)(C_{2a} - C_{2b})/(\bar{a}C_{2a} + \bar{b}C_{2b}) \qquad (20)$$
(2)

Key: (1) Weighted; (2) Weighted.

Because $T_b^* > T_a^*$, $P_b^* < P_a^*$, $\bar{a} < 1$ and $C_{2a} > C_{2b}$, it is not difficult to see from formulas (19) and (20) that $\Delta T_{weighted} > 0$ and $\Delta P_{weighted} < 0$. This is mainly because the trail region flow speed is small and the weighting corresponding to the mass mean time is relatively small. However, the mean time, i.e. the isobaric mean time, is actually on the high side for the weighting of this section. As a result, under the condition of $T_b^* > T_a^*$, T_H^* is caused to be on the high side. On the contrary, under conditions of $P_b^* < P_a^*$, P_H^* tends to be low.

In Korostelov's report, after analyzing a triangular profile, he thought that when weighting was unsuitable the opposite conditions would appear, i.e. that the total temperature would tend to be low and the total pressure high. This clearly differs from the results discussed above, and for this reason, further analysis was carried out.

Korostelov, in analyzing the triangular profile, recommended the following conditions: $z = 0 \sim a$, $\bar{z} = 0 \sim \bar{a}$, $C_{2a} = C_a$, $P^a = P_a^*$; $z = a \sim h_2$, $\bar{z} = \bar{a} \sim 1$, $C_{2a} = C_b = 0$, $P^a = P_b^*$; $P_a^* = P_a + \rho C_a^2/2$, $P_b^* = P_b + \rho C_b^2/2$, $P_a = P_b$. By substituting these conditions into formula (20), the same formula as in the above paper is obtained.

$$\Delta \overset{}{\overline{P_\mathscr{E}}} = (1-\bar{a})(P_b^* - P_a^*) = (1-\bar{a})(u^2 - C_a^2)\rho/2$$
(1)

Key: (1) Weighted.

Because $\bar{a} < 1$, when circular velocity is $u > C_a$, it can happen

56

that $\Delta P_{\text{weighted}} > 0$, i.e. the total pressure value tends to be high. For the same reason, the total temperature measured value tends to be low. It appears that this conclusion is correct. Furthermore, under conditions of static pressure equivalence, $C_b = u > C_a$ which implies that $P_b^* > P_a^*$, and that the total pressure of the trail region is instead higher than the main stream region's total pressure. Naturally, these conditions could actually not occur. For this reason, it can be stated with certainty that because weighting is unsuitable, the total temperature measured value behind the rotor tends to be high and the total pressure tends to be low.

Using formulas (19) and (20) to extract the partial derivative of $\bar{b}$, and taking into consideration $\bar{a} = 1 - \bar{b}$, we can obtain

$$\partial \Delta \overset{(1)}{T_\text{w}}/\partial \bar{b} = [\bar{b}(C_{2\text{a}} - C_{2\text{b}}) + (\bar{a} - \bar{b})](T_\text{b}^* - T_\text{a}^*)(C_{2\text{a}} - C_{2\text{b}}) \qquad (21)$$

$$\underset{(2)}{\partial \Delta P_\text{w}/\partial \bar{b}} = [\bar{b}(C_{2\text{a}} - C_{2\text{b}}) + (\bar{a} - \bar{b})](P_\text{b}^* - P_\text{a}^*)(C_{2\text{a}} - C_{2\text{b}}) \qquad (22)$$

Key: (1) Weighted; (2) Weighted.

It is thus evident that the weighted errors differ with $\bar{b}$, and are largest when $\bar{b}^2(C_{2\text{a}} - C_{2\text{b}}) = (\bar{b} - \bar{a})$.

When $\bar{b}$ is relatively thin (fig. 3a), the dynamic response errors of the total temperature and total pressure are respectively:

$$\underset{(1)}{\Delta T_\text{w}} = \frac{\tau}{t_\text{r}}(T_\text{b}^* - T_\text{a}^*)(1 - e^{-t/\tau})[(e^{-t/\tau} - e^{-t/\tau}) - 1] \qquad (23)$$

$$\underset{(2)}{\Delta P_\text{w}} = \frac{\tau_\text{p}}{t_\text{r}}(P_\text{b}^* - P_\text{a}^*)(1 - e^{-t/\tau})[(e^{-t/\tau} - e^{-t/\tau}) - 1] \qquad (24)$$

Key: (1) Response; (2) Response.

When $\bar{b}$ is relatively thick (fig. 3b), the dynamic response errors of the total temperature and total pressure are respectively:

57

$$\Delta T_a = \frac{\tau}{t_s}(T_b^* - T_a^*)(1 - e^{-t/\tau})[1 - (e^{-t/\tau} - e^{-t/\tau})] \qquad (25)$$

$$\Delta P_a = \frac{\tau_p}{t_s}(P_b^* - P_a^*)(1 - e^{-t/\tau})[1 - (e^{-t/\tau} - e^{-t/\tau})] \qquad (26)$$

Key: (1) Response; (2) Response.

Because $e^{-t/\tau} < 1, \; e^{-t/\tau} < 1;\; 1 > (1 - e^{-t/\tau}) > 0,\; 1 > (1 - e^{-t/\tau}) > 0;\; [(e^{-t/\tau} - e^{-t/\tau}) - 1] = [e^{-t/\tau}(1 - e^{-t/\tau}) - 1] < 0,\; [1 - (e^{-t/\tau} - e^{-t/\tau})] = [1 - e^{-t/\tau}(1 - e^{-t/\tau})] > 0;\; T_b^* > T_a^*, P_b^* < P_a^*.$, therefore we know from formulas (23), (24), (25) and (26) that:

When $\bar{b}$ is relatively thin, $\Delta T_{response} < 0$ and the temperature tends to be low; when $\Delta P_{response} > 0$, the pressure tends to be high.

When $\bar{b}$ is relatively thick, $\Delta T_{response} > 0$ and the temperature tends to be high; when $\Delta P_{response} < 0$, the pressure tends to be low. This is mainly because of the inertia of the probe which can neither jump nor fall sharply with it. As for the total temperature, the insufficient part of the jump is greater than the surplus part of the sharp drop when $\bar{b}$ is relatively thin; when $\bar{b}$ is relatively thick, it is smaller than the insufficient part of the sharp drop. The respective values, therefore, tend to be lower and higher. The opposite is true for total pressure.

The formulas also show that the dynamic response errors are proportional to $\tau/t_s = f_s/f_\tau$. Therefore, in order to reduce dynamic response errors, a small inertia was used; the probe with the relatively large cut-off frequency f_τ was extremely advantageous. Because $t_s = 60/(nz)$, the rotor blade number increases and the rotational speed accelerates. As $(T_b^* - T_a^*)$ and $(P_b^* - P_a^*)$ enlarge, the corresponding dynamic response errors also increase.

To summarize, in carrying out measurements behind the rotor, the total temperature measured value tends to be high and

the total pressure measured value tends tends to be low because weighting is unsuitable. Because of the inertia of the probe, total temperature is lower and total pressure is higher when $\bar{b}$ is thin; when $\bar{b}$ is thick, total temperature is higher and total pressure is lower. Rotation state errors which cause the measured values to be high or low should be concretely analyzed according to actual conditions.

For different rotors, if their $(T_b^* - T_a^*)$ and $(P_b^* - P_a^*)$ are relatively large, the rotor blade number is relatively large and the corresponding errors are relatively large. As for rotors which are the same, their rotation state errors will not only differ with the position of the radial but also change with the rotational speed and rate of flow.

If a compressor is operating at high efficiency and the probe response is slow, when the dynamic response errors occupy a main position, the total temperature measured value will be low and the total pressure will be high. However, when the compressor is close to stalling, i.e. when $\bar{b}$ is relatively thick, the total temperature will tend to be high and the total pressure will tend to be low. Figure 4 shows two methods of measuring the rotor's temperature rise: one is the temperature rise ΔT_m determined by a torsion gauge. It can approximately be regarded as $(T_m^* - T_0)$. The other method is to use seven ring surfaces of a copper-constantan thermocouple parallel to the airflow and with a diameter of 0.13mm located in the 0.4b area behind the rotor to determine the rotor's temperature rise ΔT_t. If blockage errors are neglected, $\Delta T_t = T_{Hj} - T_0$. Their error value $(\Delta T_t - \Delta T_m)$ is then the rotation state error $\Delta T_{rotation}$. Obviously, $\Delta T_{rotation}$ decreases with the rate of flow and increases with the trail relative thickness $\bar{b}$. The laws of change for the gradual increase from negative to positive are in complete agreement with the above anaysis.

The rotation state error equation cannot only be used for the qualitative analysis of rotation state errors but it can also be used to carry out quantitative calculations and as a guide for the design of the test system. The compressor rotor described below is used as an example:

Altogether a compressor has thirty moving blades and rotational speed n=10700 rotations/min. Its flow field behind the blade row is as shown in fig. 3a. T_a^*=238K, T_b^*=248K, T_0=273K, C_{2a}=93m/sec, C_{2b}=77m/sec, $\bar{a}$=0.7 and $\bar{b}$=0.3. The thermocouple's time constant τ=0.5 sec. We know from formula (19) that the weighted error of the total temperature is:

$$\Delta T_{\text{加}}^{(1)} = 0.7(1 - 0.7)(284 - 283)(93 - 77)/(0.7 \times 93 + 0.3 \times 77) = 0.04\text{℃}$$

$$\Delta T_{\text{加}}/\Delta T_{\text{k}} = 0.04/(283 - 273) = 0.4\%$$

(2)

$$t_s = 60/(10700 \times 30) = 1.87 \times 10^{-4} \text{秒}(3)$$

$$t_b = t_s \times \bar{b} = 1.87 \times 10^{-4} \times 0.3 = 5.61 \times 10^{-5} \text{秒}(4)$$

Key: (1) Weighted; (2) Weighted; (3) Seconds; (4) Seconds.

We know from formula (23) that the dynamic response error of the total pressure is:

$$\Delta T_{\text{响}}^{(1)} = \frac{0.5}{1.87 \times 10^{-4}} (284 - 283)(1 - e^{-5.61 \times 10^{-5}/0.5})[(e^{-5.61 \times 10^{-5}/0.5})$$

$$- e^{-1.87 \times 10^{-4}/0.5}) - 1] = -0.3\text{℃}$$

$$\Delta T_{\text{响}}^{(2)}/\Delta T_k = -3\%.$$

$$\Delta T_{\text{旋}} = \Delta T_{\text{加}} + \Delta T_{\text{响}} = 0.04 - 0.3 = -0.26\text{℃}. \quad \Delta T_{\text{旋}}/\Delta T_k = -2.6\%.$$

(3)   (4)   (5)   (6)

Key: (1) Response; (2) Response; (3) Rotation; (4) Weighted; (5) Response; (6) Rotation.

If we only determine a situation when $\bar{b}$ is relatively thin, for example when recording the design state performance, the rotation state error equation can be used to find the desired $\Delta T_{\text{rotation}}$=0. The corresponding probe should have a large

60

time constant. For the above example, $\Delta T_{weighted}=0.04°C$, and to cause $\Delta T_{rotation}=0$, from formula (8) we know that $\Delta T_{response}= -0.04°C$. By substituting this into formula (23), we can derive $\tau=0.05$ sec. When a thermocouple of $\tau=0.05$ sec. is used to determine the temperature rise of the compressor rotor under this given condition, the weighted errors of the total pressure and the dynamic response errors are cancelled out and $\Delta T_{rotation}=0$.

III. A METHOD FOR RAISING MEASUREMENT ACCURACY BEHIND ROTORS

Rotation state errors and blockage errors are both system errors. In order to raise measurement accuracy behind rotors, a modified or controlled method can be used. The main procedure for reducing rotation state errors and blockage errors usually has:

1. Corrected design probe

In order to reduce dynamic response errors and blockage errors, a small probe should be used as much as possible under conditions that fully ensure strength and rigidity. Usually, the probe's cut-off frequency should be $f_\tau=1/2\pi\tau < f_{signal}/10$. By using inertia compensation, the response of the testing system can be effectively raised. If the condition where $\bar{b}$ is relatively thin is only used to determine the design state, we can rely on the equation of rotation state error to select a suitable time constant to cause $\Delta T_{response}$ and $\Delta T_{weighted}$ (or $\Delta T_{weighted}$ and $\Delta T_{rotation}$) to cancel eachother and thus raise measurement accuracy. The aerodynamic blockage ratio should determine its upper limit based on the allowable error which is generally less than 6%. Using a streamline support, "L" shaped structure etc., we can effectively reduce the aerodynamic ratio. When measuring the various parameters behind the

rotor, it is usually advantageous to use a multibranched small single parameter probe of a circular dispersion point to decrease the aerodynamic blockage errors. A combination probe is suitable for use where circular fields are not homogeneous. It is suitable to use a raked shaped combination probe when the position of the radial gradient of the blade tip, blade root etc. is relatively large. If it is only used in places where the average mid radius and other radial gradients are relatively small, it is suitable to use a comb shaped combination probe to reduce aerodynamic blockage.

2. Justified distribution points

The measurement of the section's mean parameters should be realized by the fewest test points arranged according to flow field characteristics. Because each test point behind the rotor is effected by the mean working parameters of the rotor on the relative flux, only one or very few test points can be placed along the perimeter behind the rotor when the inlet flow fields are relatively homogeneous. The axial position of the test points is usually suggested as 0.2-1.5b in the literature. Here, we used the relative measurement of chord length b to show that axial positioning is possibly because chord length is a main structural parameter of the rotor blade. However, chord length and error really have no intrinsic relationship. From the point of view of error, it is suitable to determine the aerodynamic blockage ratio, if conditions permit, on the basis of permissable error and then determine the axial position on the basis of the structural measurements of the rotor and probe.

3. By using displacement mechanisms (rotation, translation and swing) and by selecting a measurement representative point, aerodynamic blockage can be effectively reduced.
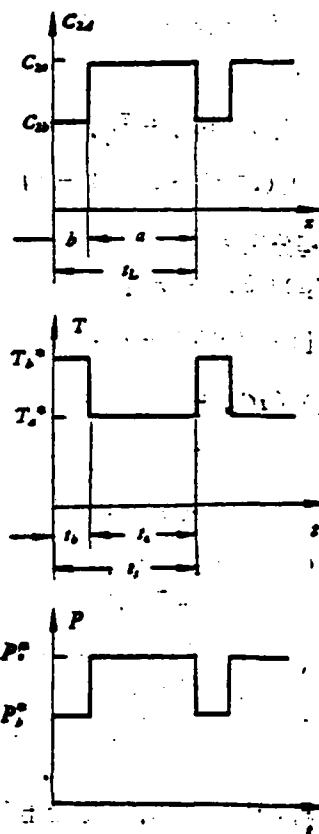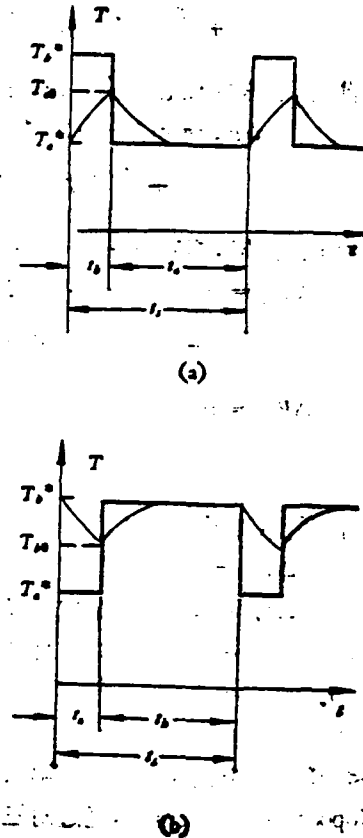
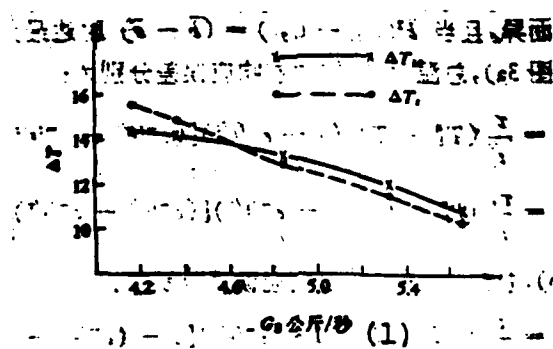Fig. 2

(a)

(b)

Fig. 3

Fig. 4

Key: (1) Kg/sec.

References

[1] Turbine Testing Task Group (Northwestern Industrial University, Xindu Machine Factory), Measurement and Analysis of Turbojet Full Flow Process Parameters, Journal of Engineering Thermophysics, 1,2,1980.

[2] Bruce V. Johnson, Henry V. Marman, John A. Brent and Richard M. Hooper: Measurement of Instantaneous Air Angle and Total Temperature Fluctuations Behind Transonic Compressor Rotors, Instrumentation for Airbreathing Propulsion, The MIT Press: Cambridge, Massachussetts, and London, England, 1973.

[3] L.N. Krause, T.J. Dudzinski and R.C. Johnson, Total Pressure Averaging in Pulsating Flows, Instrumentation for Airbreathing Propulsion, The MIT Press: Cambridge, Massachussetts and London, England, 1973.

END

FILMED

10-83

DTIC